Journal of Computational Physics 229 (2010) 6644–6662

Contents lists available at ScienceDirect

Journal of Computational Physics

journal homepage: www.elsevier.com/locate/jcp

Absorbing boundary conditions for scalar waves in anisotropic media. Part 2: Time-dependent modeling

Siddharth Savadatti, Murthy N. Guddati *

Department of Civil, Construction and Environmental Engineering, North Carolina State University, Raleigh, NC 27695-7908, United States

ARTICLE INFO

Article history:
Received 19 March 2010
Received in revised form 19 May 2010
Accepted 20 May 2010
Available online 26 May 2010

Keywords:
Wave propagation
Perfectly matched layers
Group velocity
Rational approximation
Well-posedness
Accuracy

ABSTRACT

With the ultimate goal of devising effective absorbing boundary conditions (ABCs) for general anisotropic media, we investigate the well-posedness and accuracy aspects of local ABCs designed for the transient modeling of the scalar anisotropic wave equation. The ABC analyzed in this paper is the perfectly matched discrete layers (PMDL), a simple variant of perfectly matched layers (PML) that is also equivalent to rational approximation based ABCs. Specifically, we derive the necessary and sufficient condition for the well-posedness of the initial boundary value problem (IBVP) obtained by coupling an interior and a PMDL ABC. The derivation of the reflection coefficient presented in a companion paper (S. Savadatti, M.N. Guddati, J. Comput. Phys., 2010, doi:10.1016/j.jcp.2010.05.018) has shown that PMDL can correctly identify and accurately absorb outgoing waves with opposing signs of group and phase velocities provided the PMDL layer lengths satisfy a certain bound. Utilizing the well-posedness theory developed by Kreiss for general hyperbolic IBVPs, and the well-posedness conditions for ABCs derived by Trefethen and Halpern for isotropic acoustics, we show that this bound on layer lengths also ensures well-posedness. The time discretized form of PMDL is also shown to be theoretically stable and some instability related to finite precision arithmetic is discussed.

1. Introduction

Many wave propagation problems defined on physically unbounded domains can be divided into two regions; the interior and the exterior, with the interface between them termed the computational boundary. The interior is a small bounded region where the solution to the governing equations is sought while the exterior is the rest of the unbounded domain whose effect on the interior is required *only* at the computational boundary. The computational boundary is a boundary introduced solely for computational purposes and should be distinguished from physical boundaries. Since the solution to the governing equations is not required in the exterior, the computational domain can be restricted to just the interior by specifying appropriate absorbing boundary conditions (ABCs) at the computational boundary.

ABCs are thus used to replace a 'physical' model by an equivalent 'computational' model. The physical model consists of the interior and exterior governing equations, along with initial conditions (ICs) and physical boundary conditions (BCs) defined on the physical domain (interior + exterior). The computational model consists of the interior governing equations, ICs, physical BCs and ABCs defined on the computational domain (interior + computational boundary). Both these systems are initial boundary value problems (IBVPs) and will henceforth be referred to as 'physical IBVP' and 'computational IBVP', respectively. ABCs can thus be viewed as additional constraints on the physical IBVP that limit (or expand) the space of exist-

* Corresponding author. Tel.: +1 919 515 7699; fax: +1 919 515 7908.
E-mail address: murthy.guddati@ncsu.edu (M.N. Guddati).

0021-9991/$ - see front matter © 2010 Elsevier Inc. All rights reserved.
doi:10.1016/j.jcp.2010.05.017

ing solutions. If the constraints are too restrictive, all valid solutions of the physical IBVP might be excluded rendering the computational IBVP unsolvable. If they are too lax, spurious, unphysical solutions might be admitted rendering the computational IBVP inaccurate. Hence, it is essential to ensure that the ABCs used are 'appropriate'; appropriateness here being determined through the criteria of *well-posedness* and *accuracy*. Roughly speaking, well-posedness refers to the existence of a unique solution that is bounded in some way by the initial and boundary data of the computational IBVP, while accuracy refers to the close resemblance of this unique solution to the exact solution. In addition to these two, a third criterion, namely that of computational *efficiency*, is many a times required by large scale simulations [1,2].

Exact ABCs are well-posed and accurate by default, but their availability is restricted to simple exteriors with regular computational boundaries. Approximate ABCs provide acceptable accuracy and are available for more complicated problems, but their well-posedness is not guaranteed. For large scale simulations, however, exact ABCs are prohibitively expensive; this necessitates the use of approximate ABCs. Even amongst approximate ABCs, those containing nonlocal spatial and temporal operators (global ABCs) are unsuitable for large scale problems and hence local ABCs are preferred [1,2]. The most popular local ABCs currently available are rational ABCs and perfectly matched layers (PMLs) [3]. Rational ABCs approximate the exact stiffness of an exterior (or associated dispersion relation) with rational functions of varying orders; Lindman [4], Engquist and Majda [5,6], Bayliss and Turkel [7] and Higdon [8] were their early developers followed by many others [2]. Initial numerical implementations of rational ABCs were restricted to low orders but later auxiliary variable formulations provided practical high order rational ABCs [9]. The other popular local ABC, the PML, is a 'special' absorbing medium that uses complex coordinate stretching to dampen out (or decay) propagating waves without creating artificial reflections at the computational boundary. First introduced by Bérenger [11] and closely followed by the complex coordinate stretching viewpoint provided by Chew et al. [12–14], PMLs are now available in split and unsplit forms with variations like the conformal PML [15], complex frequency shifted PML (CFS-PML) [16], convolutional PML (CPML) [17] and multiaxial PML (M-PML) [18]. Currently, both rational ABCs and PMLs are available for a wide variety of governing equations that include, among many others, Maxwell's, linearized Euler's and elastodynamic equations.

Rational ABCs tend to be more accurate than PML because the effect of the rational ABC parameters on solution accuracy is better understood (and hence more easily handled). On the other hand, ABCs based on PML have proven to be more versatile by being easily extendible to complicated exteriors [3]. The term complicated here implies material complications like heterogeneities and/or anisotropy and geometrical complications like corners and conformal boundaries. While both local ABCs satisfy the criteria of accuracy and efficiency, neither of them is assured to be well-posed *per se*. The development of both these ABCs is fraught with examples of seemingly reasonable formulations that have been found to lack well-posedness in one sense or another e.g. see [19,20]. In fact, proving well-posedness (or stability) of newly formulated ABCs is now *de rigueur* e.g. see [5,6,8,21–33]. Studies focusing solely on well-posedness issues have been rare with some accessible papers being by Higdon [34], Trefethen et al. [35], Bécache et al. [26] and Appelö et al. [36]. The references within these papers can be used to get a more comprehensive review of previous works. While the mathematical well-posedness theories are well developed today and most of their physical implications have been understood [34], their application to specific governing equations is not always straightforward; especially for complicated media.

One of the challenges to devising well-posed local ABCs for complicated (anisotropic and/or inhomogeneous) media comes from the well-posedness criterion imposed on propagating waves. Well-posedness requires that an ABC should not admit propagating modes travelling into the interior (incoming modes) in the absence of outgoing modes and sources on the boundary [34]. This makes physical sense in as much as an ABC should not allow spontaneous emission of energy into the interior without interior or boundary excitation [35]. While propagating waves are distinguished into incoming and outgoing waves depending on their group velocity, rational ABCs and PML have both been traditionally formulated to absorb waves depending on their phase velocities. This dependence on phase velocities (instead of group velocities) does not affect simple media where the phase and group velocities are always of the same sign (e.g. homogeneous isotropic media) and hence ABC formulations for simple media have turned out to be well-posed. In fact, it has been shown that a condition necessary for stability of PML (a concept related to well-posedness in the sense of providing bounds for solutions) is the absence of wave modes with phase and group velocities of differing signs [26]. Recognizing the fact that many anisotropic and/or inhomogeneous media admit such wave modes, much recent research has been focused on developing techniques that result in well-posed (or stable) local ABCs for such media. A scalar anisotropic medium whose principal material axis is tilted with respect to the coordinate axis is a simple example of a medium that allows wave modes with differing phase and group velocity signs (see Sections 2.2 and 2.3). A similar challenge, arising from the existence of wave modes with inconsistent phase and group velocity signs, has already been recognized in the cases of anisotropic electromagnetism, advective acoustics and anisotropic elastodynamics, e.g. [24–33]. Most of these studies approach the well-posedness issues from a PML viewpoint and, for the particular case of advective acoustics, all of them specify linear space–time transformations that nullify the inconsistencies in phase and group velocity signs. Moreover, many of these studies model the problem as an initial value problem (IVP) and deal with the continuous form of the ABC prior to discretization. However, actual implementations of these ABCs are discretized IBVPs and it is not entirely clear how their behavior can be inferred from the continuous IVP results.

In this paper, we consider well-posedness from a rational ABC point of view and hence deal with IBVPs. Moreover, the ABC chosen for this purpose is the perfectly matched *discrete* layer (PMDL) [37–39] that is inherently discrete. We provide a necessary and sufficient criterion for well-posedness of PMDL, when it is used as an ABC for the scalar anisotropic wave equation. In fact, this criterion is also sufficient for accuracy and is the same as the accuracy condition developed for the time

harmonic case in [40]. In essence, we prove that the parameters of PMDL (its layer lengths), need to satisfy a simple bound to exclude all ill-posed (and none of the well-posed) IBVPs resulting from the use of PMDL BCs while accurately modeling an unbounded domain governed by the scalar anisotropic wave equation. Also, we deal with strong well-posedness; even though weak well-posedness is generally sufficient for constant coefficient problems, more realistic varying coefficient problems can be well-posed only when their 'frozen' coefficient counterparts are strongly well-posed. It is hence necessary to ensure the strong well-posedness of constant coefficient problems and we do this by utilizing the well-known well-posedness theory of Kreiss [41,42]. The well-posedness criterion derived here, solely from the viewpoint of rational ABCs, bears similarity to the ones derived through coordinate transformations of PML and other ABCs in [21–33] even though the rational ABC we use for this purpose *does not* require any coordinate transformation to be enforced. This similarity is not too surprising because of the link shown to exist between rational ABCs and PML by Asvadurov et al. [43]. This link can be used to view PMDL as particularly efficient versions of PML where the perfectly matching property is preserved even after discretization making the analysis presented here meaningful to other rational ABCs and PML in general. Moreover, the absence of any coordinate transformations makes the PMDL ABC more amenable to extensions involving layered media. The details of the PMDL formulation can be found in [44] and are summarized in Section 2.4.

In this paper we deal with well-posedness and accuracy issues of a continuous interior (but discretized exterior) with a straight computational boundary. Moreover, accuracy considerations here are limited to propagating waves only. As such, interior discretization errors, corners, curved computational boundaries, loss in accuracy due to neglecting the treatment of evanescent waves and treatment of numerical instabilities related to finite precision arithmetic are outside the scope of this paper. It should be noted that the above restrictions are imposed to make the problem more tractable; they are not, with the exception of curved boundaries, due to any limitations of the PMDL formulation. Numerically stable PMDLs, capable of handling both propagating and evanescent waves for scalar isotropic media have already been implemented on domains with convex polygonal corners in [37–39]. As such, this paper can be considered as the necessary first step towards a complete PMDL implementation for anisotropic media.

The outline of the rest of the paper is as follows. Preliminaries related to scalar anisotropic wave equation are presented in Section 2 followed by a discussion of the challenges inherent in designing well-posed and accurate ABCs for such equations. A brief review of the formulation of PMDL is also presented in the same section. Section 3, which is *necessary* to understanding the results of this paper, contains a summary of the PMDL approximation properties derived in [40] and states the condition sufficient for accuracy of PMDL. Section 4 contains a statement of the well-posedness criterion and the derivation of a condition that is both necessary and sufficient for well-posedness of PMDL. Numerical stability issues are presented in Section 5 with numerical experiments presented in Section 6. Section 7 contains a summary and conclusions.

2. Preliminaries

2.1. Model problem

The ultimate aim of this paper is to provide a practical ABC for the scalar anisotropic wave equation. To this end, we choose the simplest possible boundary in two dimensions: a straight edge without corners. Fig. 1 (left) shows such a boundary ($x = 0$) and the model problem shown therein consists of replacing the exact full-space by a left half-space (interior) along with an ABC that simulates the effect of the right half-space (exterior). The interior and exterior in Fig. 1 (left) are given by $x < 0$ and $x > 0$ respectively.

2.2. Scalar anisotropic media

We consider the scalar wave equation in two dimensions $(x - y)$ given by,

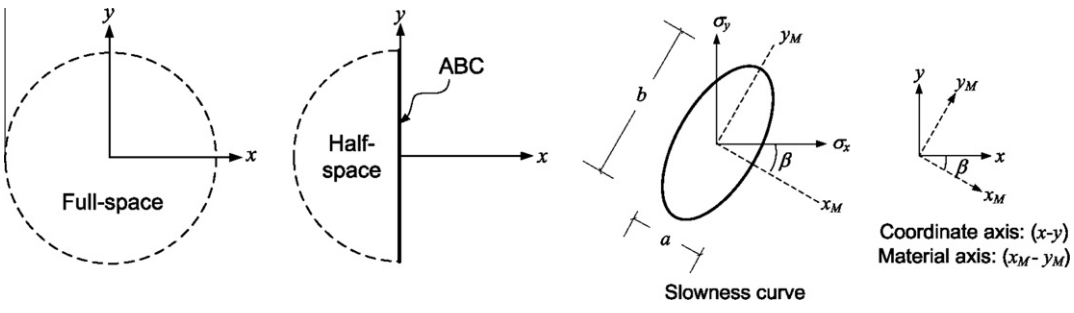

Fig. 1. Left: the model problem consists of replacing a full space by a left half-space and an efficient ABC that is both accurate and well-posed for a scalar anisotropic medium. Right: global coordinate and material axes along with a typical slowness diagram for $(\sigma_x, \sigma_y) \in \mathbb{R}$. Note that the principal material axes (x_M, y_M) are shown on the ellipse just for reference.

$$A\frac{\partial^2 u}{\partial x^2}+B\frac{\partial^2 u}{\partial y^2}+C\frac{\partial^2 u}{\partial x\partial y}-\frac{\partial^2 u}{\partial t^2}=0, \tag{1}$$

where the three independent parameters A, B, C define the material properties of the medium and can be easily obtained by coordinate stretching and rotation of the isotropic wave equation. Eq. (1), e.g. arises in the study of anti-plane shear waves in transversely isotropic elastic media, where the parameters A, B, C are functions of shear moduli, density and orientation of principal material axes of the medium. Similar scalar equations arise in the study of electromagnetism and advective acoustics. Fourier transforming (1) in y, t with the dualities $\partial/\partial y \leftrightarrow ik_y$, $\partial/\partial t \leftrightarrow -i\omega$, results in a dispersion relation in terms of horizontal slowness ($\sigma_x = k_x/\omega$) and vertical slowness ($\sigma_y = k_y/\omega$),

$$-A\sigma_x^2 - B\sigma_y^2 - C\sigma_x\sigma_y + 1 = 0. \tag{2}$$

For $(\sigma_x, \sigma_y) \in \mathbb{R}$, (2) represents an ellipse in the slowness space defined by its semiminor axis (a), semimajor axis (b) and angle of tilt (β) with respect to the $x-y$ axis as shown in Fig. 1 (right). The parameters a, b represent the material properties along $x_M - y_M$; e.g. if the medium has shear moduli μ_{x_M}, μ_{y_M} and density ρ, we have $1/a = \sqrt{\mu_{x_M}/\rho}$ and $1/b = \sqrt{\mu_{y_M}/\rho}$ representing the wave velocities along $x_M - y_M$. Simple coordinate transformations yield:

$$A = \left(\frac{\cos\beta}{a}\right)^2 + \left(\frac{\sin\beta}{b}\right)^2, \quad B = \left(\frac{\cos\beta}{b}\right)^2 + \left(\frac{\sin\beta}{a}\right)^2, \quad C = \sin 2\beta\left(\frac{1}{a^2}-\frac{1}{b^2}\right). \tag{3}$$

For later reference, we need the traction on the computational boundary ($x = 0$). The traction components in $x_M - y_M$ directions are $(a^{-2})\partial/\partial x_M$, $(b^{-2})\partial/\partial y_M$. These can be transformed through the usual second order tensor transformations to get into the traction components in $x-y$:

$$T_x : A\frac{\partial u}{\partial x} + (C/2)\frac{\partial u}{\partial y}, \quad T_y : B\frac{\partial u}{\partial y} + (C/2)\frac{\partial u}{\partial x}. \tag{4}$$

Precisely, T_x, T_y are the traction components on surfaces perpendicular to x, y axis. Without loss of generality, we consider $b \geqslant a > 0$, $\beta \in [-\pi/2, \pi/2)$ and this results in,

$$A > 0, \quad B > 0, \quad 4AB - C^2 > 0. \tag{5}$$

Variations of the three material properties A, B, C result in three kinds of slowness diagrams representing isotropic, untilted anisotropic and tilted anisotropic media as shown in Fig. 2. Note that henceforth σ_x will be represented on the vertical axis (as in Fig. 2).

For a given $\sigma_y \in \mathbb{R}$, (2) allows both propagating ($\sigma_x \in \mathbb{R}$) and evanescent modes ($\sigma_x \notin \mathbb{R}$) where each propagating wave mode is associated with a phase velocity (c_{px}) and a group velocity (c_{gx}) in the x-direction defined by:

$$\begin{aligned} c_{px} &= \frac{\omega}{k_x} = \frac{1}{\sigma_x}, \\ c_{gx} &= \frac{\partial\omega}{\partial k_x} = \frac{Ak_x + Ck_y/2}{\omega} = A\sigma_x + \frac{C\sigma_y}{2}. \end{aligned} \tag{6}$$

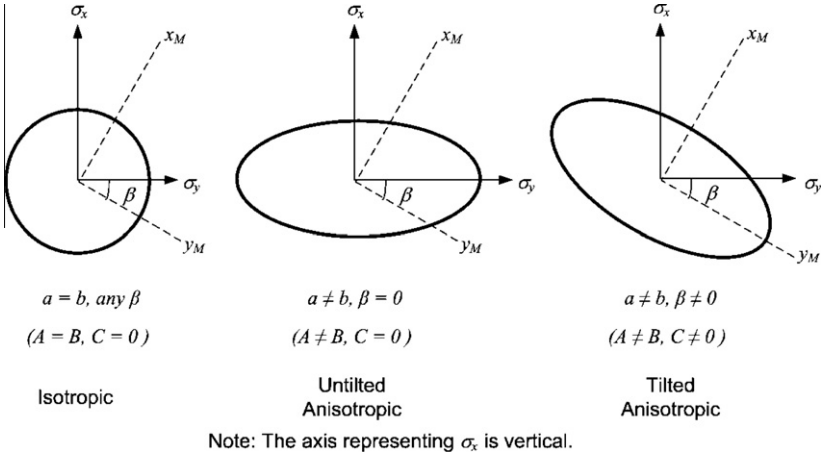

Fig. 2. Representative slowness diagrams for the three kinds of media governed by a scalar wave equation. Only slowness diagram for propagating waves is shown i.e. $(\sigma_x, \sigma_y) \in \mathbb{R}$. Note that the principal material axes (x_M, y_M) are shown on the ellipse just for reference.

It is known that while c_{px} represents the apparent velocity of propagation, c_{gx} represents the true velocity of energy propagation in the x-direction. For the rest of the paper, the terms 'phase velocity' and 'group velocity' will refer to c_{px} and c_{gx}, respectively with the understanding that these velocities are always in the x-direction.

2.3. ABCs: exact and approximate

For a given $\sigma_y \in \mathbb{R}$, the propagating modes ($\sigma_x \in \mathbb{R}$) allowed by the quadratic Eq. (2) can be classified in terms of c_{gx} as rightward and leftward propagating waves; their horizontal slownesses are given by,

$$\sigma_x = \frac{-C\sigma_y + \sqrt{4A - (4AB - C^2)\sigma_y^2}}{2A} : c_{gx} \geqslant 0 \text{ (rightward propagating)}, \tag{7}$$

$$\sigma_x = \frac{-C\sigma_y - \sqrt{4A - (4AB - C^2)\sigma_y^2}}{2A} : c_{gx} \leqslant 0 \text{ (leftward propagating)}. \tag{8}$$

Graphically, the propagating wave modes of (2) are represented by the ellipse in Fig. 3, where the rightward and leftward propagating waves of (7) and (8) are denoted by the solid and broken lines, respectively of the left ellipse in Fig. 3. An exact right half-space, in the absence of any sources within it, admits waves that either propagate to the right ($c_{gx} \geqslant 0$) or decay with increasing x (Im (σ_x) > 0). The equation of an ABC that exactly simulates a right half-space is thus given by,

$$\sigma_x = \frac{-C\sigma_y + \sqrt{4A - (4AB - C^2)\sigma_y^2}}{2A} : \text{exact ABC (slowness form)}, \tag{9}$$

where the square root is defined by the standard branch cut and $(\sigma_y, \omega) \in \mathbb{R}$. The slowness diagram of an exact ABC for propagating waves ($\sigma_x \in \mathbb{R}$) will thus be the solid portion of the left ellipse in Fig. 3.

Most approximate ABCs like traditional rational ABCs and PML are based on capturing positive phase velocities (and not group velocities) and hence cannot result in accurate ABCs when the signs of both these velocities are different i.e. when $c_{gx}c_{px} < 0$. Since there exist wavemodes with opposing signs of phase and group velocities in the case of scalar waves in tilted anisotropic media (see Fig. 3), implementations of ABCs with an arbitrary choice of parameters will, in general, allow modes with negative group velocities. Capturing the negative group velocity branch does not just lead to inaccuracies. One of the criteria necessary for the well-posedness of an ABC is that the ABC should not admit leftward propagating wave modes i.e. those with non-positive group velocities [34]. Hence, a typical approximate ABC, in conjunction with a left half-space (as in Fig. 1) actually results in an ill-posed problem – not just an inaccurate one. Designing well-posed approximate ABCs for interiors allowing modes with phase and group velocities of differing signs is a challenge that has attracted much current research, e.g. [23–30,32,33].

PMDL is a local ABC based on arbitrarily wide angle wave equations (AWWEs) [44] that can be considered to be a particularly efficient discretization of PML and has *no* discretization error [37]. PMDL forms the basis of this study because of its many attractive properties enumerated in [40]. Notwithstanding these merits however, well-posedness of PMDL is not assured, especially for general anisotropic and heterogeneous exteriors. The original PMDL formulation was shown to exhibit characteristics that might lead to ill-posedness and instabilities in complicated media [44]. In fact, this paper is a first step towards tackling the issue of ill-posedness due to anisotropy with the purpose of obtaining a well-posed PMDL for scalar waves in tilted anisotropic media.

2.4. PMDL: formulation

The model problem in Fig. 1 involves replacing the right half-space ($0 \leqslant x < \infty$) by an ABC. If the right half-space stiffness (or Dirichlet to Neumann map) is given by K_{exact}, the traction F_0 on the left boundary ($x = 0$) and the field variable there (u_0), are related by:

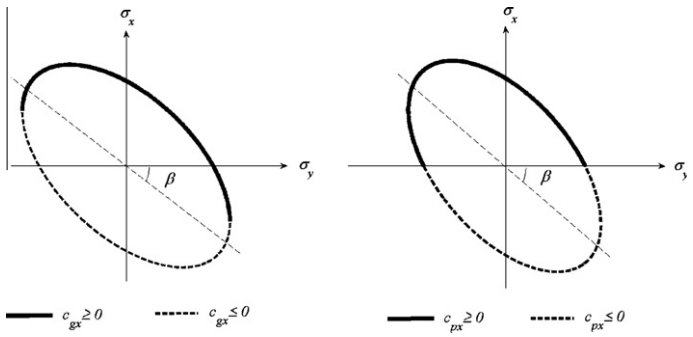

Fig. 3. A typical slowness diagram for tilted anisotropic media with the regions of positive group and phase velocities clearly demarcated.

$$F_0 = K_{\text{exact}} u_0 \ : \text{exact ABC (stiffness form)}. \tag{10}$$

Eq. (10) can be viewed as the stiffness form of the equation of an exact ABC as compared to the slowness form of (9). Substituting a mode $u = e^{i\omega(\sigma_x x+\sigma_y y-t)}$ in (4), comparing it with (10), and using (9) we get,

$$K_{exact} = -i\omega\left(A\sigma_x + \frac{C}{2}\sigma_y\right) = \frac{-i\omega\sqrt{4A-(4AB-C^2)\sigma_y^2}}{2}. \tag{11}$$

The PMDL model replaces the exterior right half-space with n ($<\infty$) mid-point integrated finite element layers of lengths $L_1,\ldots,L_n$ with a Dirichlet boundary at the end (see [40]). Using $\tilde{u}_1,\ldots\tilde{u}_{n-1},\tilde{u}_n$ to denote the values of the field variable at the right edge of each layer, the Dirichlet condition becomes $\tilde{u}_n = 0$. If $\tilde{u}_0$ is the displacement at the left edge of the n-layer PMDL model, the assembled finite element matrix takes the form,

$$\begin{Bmatrix} F_0 \\ 0 \\ 0 \\ \vdots \\ 0 \\ 0 \end{Bmatrix} = \begin{bmatrix} S_1^{11} & S_1^{12} & & & & \\ S_1^{21} & S_1^{22}+S_2^{11} & S_2^{12} & & & \\ & S_2^{21} & S_2^{22}+S_3^{11} & S_3^{12} & & \\ & & \ddots & \ddots & \ddots & \\ & & & S_{n-2}^{21} & S_{n-2}^{22}+S_{n-1}^{11} & S_{n-1}^{12} \\ & & & & S_{n-1}^{21} & S_{n-1}^{22}+S_n^{11} \end{bmatrix} \begin{Bmatrix} \tilde{u}_0 \\ \tilde{u}_1 \\ \tilde{u}_2 \\ \vdots \\ \tilde{u}_{n-2} \\ \tilde{u}_{n-1} \end{Bmatrix}, \tag{12}$$

where the element stiffness matrix for each of the n midpoint integrated layers is,

$$\mathbf{S}_j = \begin{bmatrix} S_j^{11} & S_j^{12} \\ S_j^{21} & S_j^{22} \end{bmatrix} = \frac{A}{L_j}\begin{bmatrix} 1 & -1 \\ -1 & 1 \end{bmatrix} + \frac{iC\omega\sigma_y}{2}\begin{bmatrix} 0 & -1 \\ 1 & 0 \end{bmatrix} + \frac{L_j\omega^2(B\sigma_y^2-1)}{4}\begin{bmatrix} 1 & 1 \\ 1 & 1 \end{bmatrix}, \quad j = 1,\ldots,n. \tag{13}$$

A choice of frequency dependent purely imaginary layer lengths of $L_j = 2i/\omega\sigma_{xj}$ will make the n-layer PMDL exact for a choice of slownesses $\sigma_x = \sigma_{xj}$ and these σ_{xj} are termed the n parameters of PMDL. With this, (13) becomes

$$\mathbf{S}_j = \begin{bmatrix} S_j^{11} & S_j^{12} \\ S_j^{21} & S_j^{22} \end{bmatrix} = \frac{-i\omega\sigma_{xj}A}{2}\begin{bmatrix} 1 & -1 \\ -1 & 1 \end{bmatrix} + \frac{iC\omega\sigma_y}{2}\begin{bmatrix} 0 & -1 \\ 1 & 0 \end{bmatrix} + \frac{i\omega(B\sigma_y^2-1)}{2\sigma_{xj}}\begin{bmatrix} 1 & 1 \\ 1 & 1 \end{bmatrix} \quad \text{for } (j = 1,\ldots,n). \tag{14}$$

In order to simplify later calculations (14) is written as

$$\mathbf{S}_j = -i\omega\mathbf{C}_j + \mathbf{K}_j + (i/\omega)\mathbf{R}_j, \tag{15}$$

where,

$$\mathbf{C}_j = \frac{\sigma_{xj}A}{2}\begin{bmatrix} 1 & -1 \\ -1 & 1 \end{bmatrix} + \frac{1}{2\sigma_{xj}}\begin{bmatrix} 1 & 1 \\ 1 & 1 \end{bmatrix}, \quad \mathbf{K}_j = \frac{iCk_y}{2}\begin{bmatrix} 0 & -1 \\ 1 & 0 \end{bmatrix}, \quad \mathbf{R}_j = \frac{Bk_y^2}{2\sigma_{xj}}\begin{bmatrix} 1 & 1 \\ 1 & 1 \end{bmatrix}. \tag{16}$$

Assembling the finite element matrices $\mathbf{S}_j$ and using (16), we can write (12) as,

$$\mathbf{F} = [-i\omega\mathbf{C} + \mathbf{K} + (i/\omega)\mathbf{R}]\tilde{\mathbf{u}}, \tag{17}$$

where $\mathbf{C}$, $\mathbf{K}$, $\mathbf{R}$ are finite element assemblies of element contributions $\mathbf{C}_j$, $\mathbf{K}_j$, $\mathbf{R}_j$ and $\mathbf{u} = [\tilde{u}_0,\ldots,\tilde{u}_{n-1}]^T$, $\mathbf{F} = [F_0\ 0\ldots 0]^T$. By eliminating the variables $\tilde{u}_1,\ldots,\tilde{u}_{n-1}$ from (12) we get the form,

$$F_0 = K_n\tilde{u}_0 \ : \text{approx ABC (stiffness form)}. \tag{18}$$

In essence, the n-layer PMDL model approximates only the stiffness K_{exact} and hence the displacement u_0 (both at $x = 0$) and *not* the displacement inside the half-space $u(x > 0)$. Hence we have $\tilde{u}_0 \approx u_0$ but $\tilde{u}_1,\ldots,\tilde{u}_{n-1}$ are just 'auxiliary' variables that have no physical interpretation. Comparing (18) to (10) we see that PMDL approximates the exact stiffness ($K_n \approx K_{\text{exact}}$) and the properties of this approximation are dictated solely by the choice of the n arbitrary parameters σ_{xj}. A detailed derivation of the formulation is presented in [44] with a summary in [40]. K_n is obtained by eliminating the auxiliary variables from (17) and has a rational function/continued fraction form,

$$K_n = -i\omega P_{2n,2n-2}(\sigma_y) = S_1^{11} - \cfrac{S_1^{12}S_1^{21}}{S_1^{22}+S_2^{11} - \cfrac{S_2^{12}S_2^{21}}{S_2^{22}+S_3^{11} - \ddots \cfrac{S_{n-1}^{12}S_{n-1}^{21}}{S_{n-1}^{22}+S_n^{11}}}}. \tag{19}$$

In (19), $\sigma_y = k_y/\omega$ and $P_{2n,2n-2}(\sigma_y)$ is a real rational function in σ_y of exact degrees $2n$ and $2n-2$ with $n \geqslant 1$. Comparing (19) to (11) and noting that $K_n \approx K_{\text{exact}}$, the rational approximation basis of PMDL becomes evident as,

$$P_{2n,2n-2}(\sigma_y) \approx \frac{+\sqrt{4A-(4AB-C^2)\sigma_y^2}}{2}, \tag{20}$$

and by using (20) in (9), the slowness form of PMDL becomes,

$$\sigma_x = \frac{-C\sigma_y/2 + P_{2n,2n-2}(\sigma_y)}{A} \ : \text{approx ABC (slowness form)}. \tag{21}$$

Eqs. (17) and (19) also lead to,

$$K_n = |-i\omega\mathbf{C} + \mathbf{K} + (i/\omega)\mathbf{R}|. \tag{22}$$

2.5. PMDL: approximation properties

This work is limited to propagating wave modes only i.e. we are interested in properties of ABCs that only approximate the real part of (9). Even though neglecting evanescent modes ($\sigma_x \notin \mathbb{R}$) is expected to affect the long term accuracy of the solution in the interior [10,46], and even though PMDL *can* handle evanescent wave modes [44,45], we consider this paper to be a preliminary work on rational ABCs for tilted anisotropic media and so restrict ourselves to propagating wave modes. The approximation properties of PMDL for propagating modes are best understood through the reflection coefficient that was derived in [40] and shown to have the two forms,

$$R_n = \left(\frac{\sqrt{4A-(4AB-C^2)\sigma_y^2}/2 - P_{2n,2n-2}(\sigma_y)}{\sqrt{4A-(4AB-C^2)\sigma_y^2}/2 + P_{2n,2n-2}(\sigma_y)}\right) : \text{Reflection coefficient(slowness form)}, \tag{23}$$

$$|R_n| = \left|\prod_{j=1}^{n}\left(\frac{c_{gx}-c_j}{c_{gx}+c_j}\right)\left(\frac{c_{gx}-\bar{c}_j}{c_{gx}+\bar{c}_j}\right)\right| \ (c_{gx} \geqslant 0) : \text{Reflection coefficient(group velocity form)}, \tag{24}$$

where $P_{2n,2n-2}(\sigma_y)$ is the rational function encountered in (19), and $c_j,\ \bar{c}_j$ are the reference group velocities given by,

$$\begin{aligned} c_j &= A\sigma_{xj} + (C/2)\left(\frac{-C\sigma_{xj} + \sqrt{4B-(4AB-C^2)\sigma_{xj}^2}}{2B}\right), \\ \bar{c}_j &= A\sigma_{xj} + (C/2)\left(\frac{-C\sigma_{xj} - \sqrt{4B-(4AB-C^2)\sigma_{xj}^2}}{2B}\right). \end{aligned} \tag{25}$$

c_{gx} in (24) is the group velocity of the incident wave mode that is propagating rightward and hence $c_{gx} \geqslant 0$. Defining the vertical slownesses,

$$\begin{aligned} \sigma_{yj} &= \frac{-C\sigma_{xj} + \sqrt{4B-(4AB-C^2)\sigma_{xj}^2}}{2B}, \\ \bar{\sigma}_{yj} &= \frac{-C\sigma_{xj} - \sqrt{4B-(4AB-C^2)\sigma_{xj}^2}}{2B}, \end{aligned} \tag{26}$$

for every σ_{xj} (i.e. every layer of length $L_j = 2i/\omega\ \sigma_{xj}$), the PMDL slowness interpolates the exact slowness (2) at the four points given by $(\sigma_{yj}, \sigma_{xj}), (-\sigma_{yj}, \sigma_{xj} + (C/A)\sigma_{yj}),\ (\bar{\sigma}_{yj}, \sigma_{xj})$ and $(-\bar{\sigma}_{yj}, \sigma_{xj} + (C/A)\bar{\sigma}_{yj})$. It should be noted that these four points of interpolation need not necessarily be distinct, but for every choice of σ_{xj}, there are four points of interpolation counted *with multiplicity*. A n-layer PMDL has n parameters (σ_{xj} with $j = 1 \ldots n$) and hence it has $4n$ points of interpolation in all counted with multiplicity. Detailed discussion can be found in [40].

3. Accuracy

A n-layer PMDL is considered convergent (or accurate, following the terminology in the ABC literature) if, by increasing the number of layers n, the magnitude of its reflection coefficient can be made arbitrarily small for every strictly rightward propagating wave mode, i.e.

$$\lim_{n\to\infty} |R_n(c_{gx})| = 0 \quad \forall\ c_{gx} > 0 : \text{accuracy criterion}. \tag{27}$$

The reason for the criterion (27) to be 'accurate enough' while excluding the zero group velocity mode ($c_{gx} = 0$) is stated in [40] and essentially reduces to the fact that a PMDL ABC that allows $c_{gx} = 0$ to exist in the interior ends up being ill-posed [34].

This incompatibility between being well-posed and being able to represent zero group velocity modes accurately is not unique to PMDL. A similar situation occurs between accuracy and stability of difference approximations in [47]. In fact, for the case of untilted anisotropy, $\lim_{n\to\infty}|R_n(0)| = 0$ cannot be satisfied by any existing local ABC. The calculations in [40] show that a sufficient condition for (27) to be satisfied is,

$$\sigma_{xj} > \left| \frac{C}{\sqrt{A(4AB - C^2)}} \right| \tag{28}$$

The above condition (28) has a simple geometric interpretation that is shown in Fig. 4.

The n-layer PMDL approximates the stiffness (11) by a rational function instead of approximating the horizontal slowness directly. It can be seen from (11) and (6) that the stiffness for propagating wave modes is in fact related to their group velocity as $K = -i\omega\, c_{gx}$ and hence approximating stiffness is the same as approximating group velocities. This is the reason why the PMDL reflection coefficient (24) is expressible purely in terms of group velocities and as noted in [40], the form of (24) is *key* to the derivation of the simple accuracy condition (28).

4. Well-posedness

4.1. Well-posedness of an ABC

Kreiss gave necessary and sufficient algebraic conditions for well-posedness of systems of linear hyperbolic initial boundary value problems (IBVPs) defined on a half-space [41] by specifying energy estimates depending on initial and boundary data that need to be satisfied. Well-posedness in Kreiss's sense reduces to avoiding certain ill-posed normal modes of the form $e^{ik_x x + ik_y y - i\omega t}$ where $k_y \in \mathbb{R}$ but where k_x and ω are allowed to be complex. In general, these ill-posed modes are solutions to the computational IBVP that are L_2 integrable in $x \leqslant 0$ but fail to satisfy the specified energy estimate [34]. Trefethen and Higdon have both provided useful physical interpretation of Kreiss's ill-posed normal modes in the context of ABCs for wave propagation problems [34,48]. In the case of the model problem containing an interior left half-space with an ABC at $x = 0$, ill-posed normal modes are solutions to (1) of the form $e^{ik_x x + ik_y y - i\omega t}$ with $k_y \in \mathbb{R}$ and with the (k_x, ω) pair satisfying any one of the following three criteria:

$$\begin{aligned}
&\mathrm{Im}(\omega) > 0,\ \mathrm{Im}(k_x) < 0 \text{ (modes growing exponentially in time while decaying into the interior)}\\
&\mathrm{Im}(\omega) = 0,\ \mathrm{Im}(k_x) = 0,\ c_{gx} \leqslant 0 \text{ (leftward propagating modes)}\\
&\mathrm{Im}(\omega) = 0,\ \mathrm{Im}(k_x) < 0 \text{ (evanescent modes decaying into the interior)}.
\end{aligned}$$

The first of these modes is L_2 integrable in $x \leqslant 0$ but grows exponentially in time. The second mode contains propagating waves that propagate energy into the interior ($c_{gx} < 0$) without any interior or boundary excitation. This again leads to unbounded growth in time though at a much slower rate. Physically, it is not immediately apparent why propagating waves moving tangential to the boundary (the case of $c_{gx} = 0$ for the second ill-posed mode) and evanescent modes decaying into the interior (third ill-posed mode) should result in ill-posedness. Mathematically, however, the second and third modes are limiting cases of the first mode that is clearly ill-posed. A more detailed discussion of these ill-posed modes can be found in [34]. If any of the above three modes is allowed by the interior governing equation in conjunction with the ABC, then the

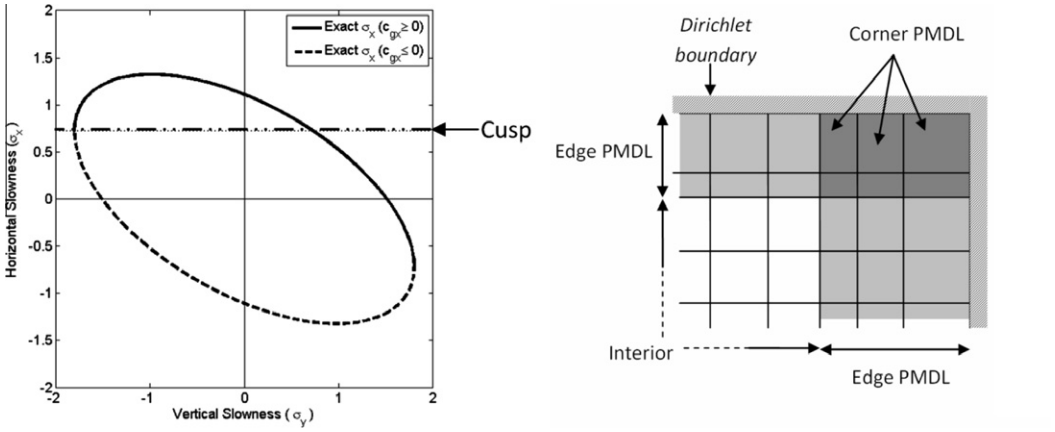

Fig. 4. Left: geometric interpretation of the sufficient condition for accuracy. The parameters of PMDL should be chosen above the horizontal line that defines the 'cusp' of the ellipse. Right: corner PMDL with parameters (layer lengths) consistent with the two edge PMDLs.

model in Fig. 1 containing a left-half space with an ABC on its boundary is ill-posed. Additionally, the exclusion of these ill-posed modes is known to be sufficient for ensuring well-posedness [34,35].

4.2. Well-posedness criterion

Trefethen and Halpern [35] provided well-posedness criterion for rational ABCs for isotropic acoustics ($A = B = 1$, $C = 0$ in (1)). In this sub-section we extend this criterion to tilted anisotropic acoustics, and state it in relation to a n-layer PMDL. In order to facilitate understanding and comparison, we reproduce the order and flow of [35] even if it leads to the restatement of a few equations.

The exact dispersion relation of (1) is:

$$-Ak_x^2 - Bk_y^2 - Ck_xk_y + \omega^2 = 0. \tag{29}$$

Eq. (29) admits two solutions for k_x given by,

$$k_x = \frac{-Ck_y + \omega\sqrt{4A - (4AB - C^2)(k_y^2/\omega^2)}}{2A}, \tag{30}$$

$$k_x = \frac{-Ck_y - \omega\sqrt{4A - (4AB - C^2)(k_y^2/\omega^2)}}{2A}. \tag{31}$$

For $(k_x, k_y, \omega) \in \mathbb{R}$, (30) represents rightward propagating waves ($c_{gx} \geqslant 0$) and (31) represents leftward propagating waves ($c_{gx} \leqslant 0$). The distinction of tangential waves ($c_{gx} = 0$) is ignored for now; it will become necessary only later. The ABC in Fig. 1 should admit rightward propagating waves ($c_{gx} \geqslant 0$), and so it approximates (30) with a rational function given by (from (21)),

$$k_x = \frac{-Ck_y/2 + \omega P_{2n,2n-2}}{A} : \text{approx ABC } (n\text{-layer PMDL}), \tag{32}$$

where $\sigma_y = k_y/\omega$ and $P_{2n,2n-2} = p_{2n}(\sigma_y)/q_{2n-2}(\sigma_y)$. Here, $p_{2n}(\sigma_y)$ and $q_{2n-2}(\sigma_y)$ are polynomials of exact degrees $2n$ and $2n-2$, respectively with $n \geqslant 1$ and with no common zeros. Multiplying (32) by $A\omega^{2n-1}q_{2n-2}(\sigma_y)$ and rearranging we get:

$$Q(k_x, k_y, \omega) = 0, \tag{33}$$

where Q is a homogeneous polynomial of degree $2n$ in the three variables k_x, k_y, ω and is given by:

$$Q(k_x, k_y, \omega) = A\omega^{2n-1}k_xq_{2n-2} + C\omega^{2n-1}k_yq_{2n-2}/2 - \omega^{2n}p_{2n}. \tag{34}$$

Eq. (33) is the dispersion relation of the n-layer PMDL. Since the rational function $P_{2n,2n-2}$ and hence p_{2n},q_{2n-2} are given by (14) and (19), their coefficients are determined by the n parameters σ_{xj}. Thus, for real parameters ($\sigma_{xj} \in \mathbb{R}$), (34) represents a polynomial with real coefficients.

It should be noted that in the previous sections, we were concerned with modes of the kind $e^{i(k_xx+k_yy-\omega t)}$ with $(k_y, \omega) \in \mathbb{R}$. However, since well-posedness is also concerned with modes growing in time, the restriction to real ω is no longer sufficient. This is suggested by the first ill-posed mode. The existence of complex ω is a result of Laplace transforms used in the derivation of these ill-posed modes [34,41]. Hence we have $k_y \in \mathbb{R}$ and $(k_x, \omega) \in \mathbb{C}$; this requires a clear definition for the square root used in (30) and (31). To facilitate comparison with [35], we define the square root in (31); the square root in (30) can be inferred accordingly.

Consider the case of $k_y = 0$ first. A natural definition of the square root branch in (31) gives $k_x = -\omega/\sqrt{A}$. For later use note that $k_x = -\omega/\sqrt{A}$ has the following implication: Im $(\omega) > 0 \Rightarrow$ Im $(k_x) < 0$. For $k_y \neq 0$, we can define the function $k_x = \left(-Ck_y - \sqrt{4A\omega^2 - (4AB - C^2)k_y^2}\right)/2A$ to be an analytic continuation of the function $k_x = -\omega/\sqrt{A}$. When Im $(\omega) \neq 0$, this continuation preserves the implication Im $(\omega) > 0 \Rightarrow Im(k_x) < 0$. When $\omega \in \mathbb{R}$, k_x can be defined as the limit obtained through Im $(\omega) \to 0^+$. The limiting process involves Im $(\omega) > 0$ and hence results in Im $(k_x) < 0$ when $|\omega| < \left(\sqrt{B - C^2/4A}\right)|k_y|$ in (31). Formally this leads to the following definition:

Definition of square root:

- For Im $(\omega) > 0$, the branch (31) refers to the analytic function $k_x = \left(-Ck_y - \sqrt{4A\omega^2 - (4AB - C^2)k_y^2}\right)/2A$ of k_y and ω obtained by analytic continuation from the values $k_x = -\omega/\sqrt{A}$ for $k_y = 0$ with Im $(k_x) < 0$.
- For $\omega \in \mathbb{R}$, k_x in branch (31) is defined by limits in the half-plane Im $(\omega) > 0$, and satisfies:
  - $Im(k_x) < 0$ if $|\omega| < \left(\sqrt{B - C^2/4A}\right)|k_y|$,
  - $k_x \in \left(-Ck_y - 2\sqrt{A}\omega[0, 1]\right)/2A$ if $|\omega| \geqslant \left(\sqrt{B - C^2/4A}\right)|k_y|$.

Similarly, for $Im(\omega) \geqslant 0$, branch (30) results in $Im(k_x) > 0$ or $k_x \in (-Ck_y + 2\sqrt{A}\omega[0,1])/2A$. The same logic can also be followed to define (30) and (31) for $Im(\omega) < 0$.

With this definition of the square root, we can immediately see that all the three ill-posed modes belong to branch (31). This is obvious for the first and third ill-posed modes because only branch (31) results in $Im(k_x) < 0$. The second ill-posed mode contains propagating wave modes that have non-positive group velocity. Propagating wave modes i.e. those with $(k_x, k_y, \omega) \in \mathbb{R}$ have group velocity given by $c_{gx} \in \sqrt{A}[-1,1]$. This can be seen by substituting (30) and (31) into the group velocity expression (31). Since branch (31) allows propagating wave modes with $k_x \in \left(-Ck_y - 2\sqrt{A}\omega[0,1]\right)/2A$, we can see that it allows modes with $c_{gx} \in \sqrt{A}[-1,0] \leqslant 0$. Since this includes all non-positive group velocities, the second ill-posed mode also belongs to branch (31). Moreover, the branch (31) does not admit any well-posed modes. All modes admitted by (31) with $Im(\omega) \geqslant 0$ are ill-posed as shown above. For $Im(\omega) < 0$, (31) results in $Im(k_x) > 0$; these modes are *not* L_2 integrable in the domain $(x \leqslant 0)$ and hence physically inadmissible in the first place. Thus the IBVP is well-posed if and only if the approximation does not contain the branch (31), i.e.

Well-posedness criterion: The model problem of Fig. 1 is well posed if and only if (34) and (29) have no mutual solutions $(k_x, k_y, \omega) \neq (0, 0, 0)$ with $k_y \in \mathbb{R}$, $\mathrm{Im}(\omega) > 0$, and k_x belonging to the branch (31).

This criterion can be rewritten solely in terms of vertical slowness σ_y and the rational approximation provided by the n-layer PMDL. For this we can assume $\omega \neq 0$; for if it is, Eq. (29) gives $k_x = \left(-C \pm i\sqrt{4AB - C^2}\right)k_y/2A$ and this with (33) implies $k_x = k_y = 0$ which is of no interest. For $k_y \in \mathbb{R}$ and $\mathrm{Im}(\omega) > 0$, the variable $\sigma_y = k_y/\omega$ lies in the set $\mathbb{C} \setminus ((-\infty, 0) \cup (0, \infty))$. Including limits $\mathrm{Im}(\omega) \to 0$, $\omega \nrightarrow 0$ amounts to letting σ_y range all over $\mathbb{C}$ with points on the two sides of the cuts $(-\infty, 0)$, $(0, \infty)$ viewed as distinct. Hence the well-posedness criteria reduces to (34) and (31) having no mutual solutions for $\sigma_y \in \mathbb{C}$. Since (34) is but a form of (32), the well-posedness criterion further reduces to:

$$\frac{-C\sigma_y - \sqrt{4A - (4AB - C^2)\sigma_y^2}}{2A} \neq \frac{-C\sigma_y/2 + P_{2n,2n-2}}{A}, \quad (\sigma_y \in \mathbb{C}): \text{ well-posedness criterion.} \tag{35}$$

Eq. (35) is the criterion for a n-layer PMDL to act as a well-posed ABC for the model problem in Fig. 1 with a tilted anisotropic interior. The above arguments from (33) till (35), except for some explanations and extensions to the case of tilted anisotropy, are straightforward extensions of the arguments presented in [35] for isotropic acoustics.

4.3. Reformulation of the well-posedness criterion

As noted before, necessary and sufficient conditions for well-posedness of general rational ABCs have been derived by Trefethen and Halpern [35] for isotropic acoustics ($A = B = 1$, $C = 0$ in (1)). These results are applicable to scalar, *untilted* anisotropic media without any modification. In this sub-section, we show that the form of the n-layer PMDL (21) is such that it will allow us to extend Trefethen and Halpern's isotropic acoustics results to tilted anisotropy. To this end, we reformulate (35) in terms of interpolation points before deriving necessary and sufficient conditions for well-posedness of PMDL.

Since $A \neq 0$, (35) is equivalent to:

$$\frac{-\sqrt{4A - (4AB - C^2)\sigma_y^2}}{2} \neq P_{2n,2n-2}, \quad \text{for } \sigma_y \in \mathbb{C}. \tag{36}$$

Using $A > 0$, $4AB - C^2 > 0$ from (5), we can divide (36) by $\sqrt{A}$ to get $-\sqrt{1 - (B - C^2/4A)\sigma_y^2} \neq P_{2n,2n-2}/\sqrt{A}$, which, with the following,

$$\begin{aligned} \tilde{\sigma}_y &= \left(\sqrt{(B - C^2/4A)}\right)\sigma_y, \\ \tilde{P}_{2n,2n-2} &= P_{2n,2n-2}/\sqrt{A}, \end{aligned} \tag{37}$$

results in the form:

$$-\sqrt{1 - \tilde{\sigma}_y^2} \neq \widetilde{P}_{2n,2n-2}(\tilde{\sigma}_y), \quad \text{for } \tilde{\sigma}_y \in \mathbb{C}. \tag{38}$$

$\widetilde{P}_{2n,2n-2}(\tilde{\sigma}_y)$, like $P_{2n,2n-2}(\sigma_y)$, is a rational function with real coefficients.

Eq. (38) can further be simplified by noting that, on $(-\infty, -1)$ and $(1, \infty)$, the inequality is always true because the left-hand side is imaginary, finite and non-zero while the right-hand side is real or infinite. Hence the well-posedness criterion reduces to,

$$-\sqrt{1 - \tilde{\sigma}_y^2} \neq \widetilde{P}_{2n,2n-2}(\tilde{\sigma}_y), \quad \text{for } \tilde{\sigma}_y \in \mathbb{C} - (-\infty, -1) - (1, \infty). \tag{39}$$

It should be remembered that (38) is still the well-posedness criterion for *tilted* anisotropic media. Since the rational function $P_{2n,2n-2}(\sigma_y)$ and hence $\widetilde{P}_{2n,2n-2}(\tilde{\sigma}_y)$ are defined by (19) and (14), the well-posedness criterion reduces to finding the parameters σ_{xj} of (14), so that (39) is satisfied. The form of (38) and (39) is the form that occurs in the well-posedness study of

isotropic acoustics and as such, those results are directly applicable to our problem. It should be noted that we were able to arrive at the form of (38) and (39) *only* because of the special form of (32) wherein the stiffness of the exact right half-space is approximated by a rational function (19) to get $K_n \approx K_{\text{exact}}$.

We now use the results derived for isotropic acoustics and reformulate (39) in terms of interpolation points. One of these results concerns a real rational function $P_{r,s}$ of exact type (r, s) with $P_{r,s}(0) \neq 0,\infty$. It has been shown in [35] (Lemma 2) that the following conditions are equivalent:

(a) $P_{r,s}(\sigma) = -\sqrt{1-\sigma^2}$ has no solutions in $\mathbb{C} - (-\infty, -1) - (1, \infty)$.
(b) $s \leqslant r \leqslant s+2$ and $P_{r,s}(\sigma) = +\sqrt{1-\sigma^2}$ has $r+s+1+\chi_{rs}$ solutions in $\mathbb{C} - (-\infty, -1] - [1, \infty)$, counted with multiplicity. Here $\chi_{rs} = 0$ if $r+s$ is odd and $\chi_{rs} = 1$ if $r+s$ is even.

In our case $P_{2n,2n-2}(\sigma_y)$ and hence $\widetilde{P}_{2n,2n-2}(\tilde{\sigma}_y)$ are real rational functions of exact type $(2n, 2n-2)$ for $\sigma_{xj} \in \mathbb{R}$. If we can show that $\widetilde{P}_{2n,2n-2}(0) \neq 0, \infty$, then (39) is precisely the statement (a) above and can hence be replaced by the equivalent statement (b). The rational function $\widetilde{P}_{2n,2n-2}(\tilde{\sigma}_y)$ already satisfies the condition $s \leqslant r \leqslant s+2$, and hence (39) becomes: For $\sigma_{xj} \in \mathbb{R}$, $+\sqrt{1-\tilde{\sigma}_y^2} = \widetilde{P}_{2n,2n-2}(\tilde{\sigma}_y)$ has $4n$ solutions in $\mathbb{C} - (-\infty, -1] - [1, \infty)$ counted with multiplicity. We can now undo the change instigated in (37) to write the above well-posedness criterion as: For $\sigma_{xj} \in \mathbb{R}$, $+\sqrt{4A - (4AB - C^2)\sigma_y^2}/2 = P_{2n,2n-2}(\sigma_y)$ has $4n$ solutions in $\mathbb{C} - (-\infty, -d] - [d, \infty)$ counted with multiplicity. Here $d = 2\sqrt{A}/\sqrt{4AB - C^2}$. An equivalent statement in terms of interpolation points is:

A n-layer PMDL is well-posed if and only if $(-C\sigma_y/2 + P_{2n,2n-2})/A$ interpolates $\left(-C\sigma_y + \sqrt{4A - (4AB - C^2)\sigma_y^2}\right)/2A$ at $4n$ points in $\mathbb{C} - (-\infty, -d] - [d, \infty)$ counted with multiplicity.

The above well-posedness criterion requires $\widetilde{P}_{2n,2n-2}(0) \neq 0, \infty$. Using (5) and (37) an equivalent requirement is $P_{2n,2n-2}(0) \neq 0,\infty$. Instead of proving $P_{2n,2n-2}(0) \neq 0,\infty$ right now, we assume it to be true and derive conditions under which the last stated well-posedness criterion is satisfied. We then show that these conditions ensure $P_{2n,2n-2}(0) \neq 0,\infty$.

It has already been stated in Section 2.5 that the n-layer PMDL exactly interpolates $4n$ points (counted with multiplicity) on the slowness curve [40]. Comparing this with the last stated well-posedness criterion, we can see that the only thing that remains to be done, is to find conditions under which all these $4n$ points are on $\left(-C\sigma_y + \sqrt{4A - (4AB - C^2)\sigma_y^2}\right)/2A$ in the required domain $\mathbb{C} - (-\infty, -d] - [d, \infty)$ and not on $\left(-C\sigma_y - \sqrt{4A - (4AB - C^2)\sigma_y^2}\right)/2A$. This is done in the following subsection.

4.4. Necessary and sufficient conditions

For clarity, we rewrite the positive and negative branches of the horizontal slowness,

$$\sigma_x = \frac{-C\sigma_y + \sqrt{4A - (4AB - C^2)\sigma_y^2}}{2A}, \tag{40}$$

$$\sigma_x = \frac{-C\sigma_y - \sqrt{4A - (4AB - C^2)\sigma_y^2}}{2A}, \tag{41}$$

and restate the well-posedness criterion obtained at the end of the previous sub-section.

Well-posedness criterion: The model problem of Fig. 1 with a scalar anisotropic medium and with a n-layer PMDL is well-posed if and only if $(-C\sigma_y/2 + P_{2n,2n-2})/A$ interpolates (40) at $4n$ points in $\mathbb{C} - (-\infty, -d] - [d, \infty)$ counted with multiplicity where $d = 2\sqrt{A}/\sqrt{4AB - C^2}$.

In Section 3 we stated the sufficient criterion for accuracy (28) by first imposing the condition of positive reference group velocities $c_j > 0,\ \bar{c}_j > 0$ at each of the $4n$ interpolation points. The condition $c_j > 0,\ \bar{c}_j > 0$, by definition, forces interpolation of the positive group velocity branch (40) and hence we expect (28) to play some role in assuring well-posedness. In-fact, we now show that (28) is *both* necessary and sufficient for satisfying the above well-posedness criterion.

Motivated by the derivation of the sufficient condition for accuracy, we first consider a choice of parameters:

$$\left|\frac{C}{\sqrt{A(4AB - C^2)}}\right| < \sigma_{xj} \leqslant \frac{2\sqrt{B}}{\sqrt{4AB - C^2}} \tag{42}$$

Using (26) and after some manipulations, the choice of (42) results in:

$$\sigma_{yj} \in (-d, d),\ \bar{\sigma}_{yj} \in (-d, d) \quad \text{where } d = 2\sqrt{A}/\sqrt{4AB - C^2}. \tag{43}$$

It can be seen from (25) that (42) ensures $c_j > 0,\ \bar{c}_j > 0$ and so we have $4n$ points of interpolation of the positive group velocity branch (40) (or equivalently (30)). Hence (42) is sufficient for well-posedness.

We next consider,

$$\sigma_{xj} > \frac{2\sqrt{B}}{\sqrt{4AB - C^2}}. \tag{44}$$

From Section 2.5, we have the usual four points of interpolation (including both positive and negative group velocity branches) $\sigma_y = \pm\sigma_{yj},\ \pm\bar{\sigma}_{yj}$. Based on (26), none of these interpolation points are real and thus they belong to $\mathbb{C} - \mathbb{R}$. We further show that none of these points can interpolate the non-positive group velocity branch (41) thus asserting that all four points interpolate the positive group velocity branch (40) with $\sigma_y \in \mathbb{C} - \mathbb{R}$.

The (σ_y, σ_x) pairs of the four interpolation points were stated in Section 2.5 to be $(\sigma_{yj}, \sigma_{xj}),\ (-\sigma_{yj}, \sigma_{xj} + (C/A)\sigma_{yj}),\ (\bar{\sigma}_{yj}, \sigma_{xj})$ and $(-\bar{\sigma}_{yj}, \sigma_{xj} + (C/A)\bar{\sigma}_{yj})$. We will consider each of these separately.

Consider the point of interpolation $(\sigma_{yj}, \sigma_{xj})$: From (44) and (26) we have Im $(\sigma_{yj}) \neq 0$. At the point of interpolation, $k_y = \omega\sigma_{yj}$, $k_x = \omega\sigma_{xj}$ and since $k_y \in \mathbb{R}$, we have Im $(\omega) \neq 0$. If Im $(\omega) > 0$, we get Im $(k_x) > 0$ (because (44) implies $\sigma_{xj} > 0$). Hence k_x cannot lie on (41) because for $k_y \in \mathbb{R}$ the negative branch of the square root has Im $(k_x) < 0$ (from the definition of square root). The same argument holds for the interpolation point $(\bar{\sigma}_{yj}, \sigma_{xj})$ with $k_y = \omega\bar{\sigma}_{yj}$.

Consider the point of interpolation $(-\sigma_{yj}, \sigma_{xj} + (C/A)\sigma_{yj})$: From (44) and (26), we have Im $(\sigma_{yj}) \neq 0$. At the point of interpolation, $k_y = \omega\ (-\sigma_{yj})$, $k_x = \omega(\sigma_{xj} + (C/A)\sigma_{yj}) = \omega\sigma_{xj} - (C/A)k_y$ and since $k_y \in \mathbb{R}$, we have Im $(\omega) \neq 0$. If Im $(\omega) > 0$, we get Im $(k_x) > 0$ (because (44) implies $\sigma_{xj} > 0$). The rest is identical to the above argument for $(\sigma_{yj}, \sigma_{xj})$ and the same holds for $(-\bar{\sigma}_{yj}, \sigma_{xj} + (C/A)\bar{\sigma}_{yj})$.

The above arguments show that, for Im $(\omega) > 0$, (44) ensures that the four points of interpolation lie in $\mathbb{C} - \mathbb{R}$ and interpolate (40). *To summarize*: The condition (42), and for Im $(\omega) > 0$ the condition (44), ensure $4n$ points of interpolation of the positive branch (40) in $(-d, d)$ and $\mathbb{C} - \mathbb{R}$, respectively. Combining (42) and (44) we see that for,

$$\sigma_{xj} > \left| \frac{C}{\sqrt{A(4AB - C^2)}} \right|, \tag{45}$$

$(-C\sigma_y/2 + P_{2n,2n-2})/A$ interpolates (40) at $4n$ points in $\mathbb{C} - (-\infty, -d] - [d, \infty)$ counted with multiplicity (again for $Im(\omega) > 0$ where applicable) and we thus have a sufficient condition for well-posedness.

To show that (45) is also necessary, the above arguments (from (42) onwards) can easily be reversed to show that $\sigma_{xj} \leqslant |C/\sqrt{A(4AB - C^2)}|$ ensures at least one interpolation of the wrong branch (41) in $\mathbb{C} - (-\infty, -d] - [d, \infty)$. For example, for $-2\sqrt{B}/\sqrt{4AB - C^2} \leqslant \sigma_{xj} \leqslant |C/\sqrt{A(4AB - C^2)}|$, we get at least one of the reference group velocities to be non-positive i.e. $c_j \leqslant 0$ and/or $\bar{c}_j \leqslant 0$ from (25). This implies at least one corresponding point of interpolation of the wrong branch. For $\sigma_{xj} < -2\sqrt{B}/\sqrt{4AB - C^2}$, we can reverse the arguments immediately following (44) using the fact that $\sigma_{xj} < 0$.

The above arguments show that (45) is *both* a *necessary* and a *sufficient* condition for satisfying the well-posedness criterion presented at the beginning of this sub-section.

We assumed $P_{2n,2n-2}(\sigma_y) \neq 0, \infty$ for $\sigma_y = 0$, in deriving the well-posedness criterion (45) (see the ending of the last subsection); this assumption can now be verified as follows. At $\sigma_y = 0,\ c_{gx} = \sqrt{A}$ from (6) and (7). Since (45) is the same as the sufficient condition for accuracy (28), based on the definition of accuracy in (27) and given that $c_{gx} = \sqrt{A} > 0$, we have $|R_n| < 1$. Since $|R_n| < 1$, based on (23), $P_{2n,2n-2}(\sigma_y) \neq 0, \infty$ for $\sigma_y = 0$.

Hence, (45) is a necessary and sufficient condition for well-posedness of a n-layer PMDL with parameters $\sigma_{xj} \in \mathbb{R}$ $(j = 1, \ldots, n)$. Since this is the same as (28), well-posedness *guarantees* accuracy. The geometric representation of (45) is shown in Fig. 4.

It was shown in [40] that (28) is a sufficient condition for accuracy. It might be possible to show that it is also necessary for accuracy in some sense. We do not bother to do this because any change in (28) will only lead to ill-posedness as (28) is already a necessary condition for well-posedness.

4.5. Relation between tilted and untilted anisotropy

We were able to arrive at the well-posedness condition (45) for tilted anisotropic media by using the results already available for isotropic acoustics. We have already noted in Section 3 and in [40], that the distinguishing characteristic of PMDL is that it approximates stiffness instead of the horizontal wave number. This characteristic is precisely the one that allows us to borrow the results from isotropic acoustics and apply them to tilted anisotropy. The two properties that distinguish tilted anisotropy from isotropy are obviously the anisotropy $(A \neq B)$ and the tilt $(C \neq 0)$ as shown in Fig. 2. Untilted anisotropy can be easily converted to isotropy by a simple scaling of variable as in (37). Hence, if we wish to somehow connect tilted anisotropy to isotropy, the difficulty mainly lies in converting tilted anisotropy to untilted anisotropy.

The exact horizontal slowness (9) represents a tilted ellipse in (σ_y, σ_x) space for $A \neq B$ and $C \neq 0$. However, the exact stiffness given by (11) represents an *untilted* ellipse in $(\sigma_y, iK/\omega)$ space. Since the current PMDL approximates stiffness (or iK/ω to be more precise) by a rational function $P_{2n,2n-2}$ (20), we are in essence approximating an *untilted* ellipse by a rational function even though we are dealing with tilted anisotropic media. But approximating untilted ellipses by rational functions is pre-

cisely what occurs in rational approximations of untilted anisotropy [35]. Hence, approximating stiffness in general, and the form of our PMDL (19) in particular, provides a natural connection between tilted and untilted anisotropy. This explains our ability to use the well-posedness results of isotropic acoustics.

Well-posedness (or stability) of PML for convective acoustics with uniform parallel and oblique mean flow (dispersion relation of shifted and/or tilted ellipse) has been possible due to linear variable transformations (see [23–30,32]). Among other things, such variable transformations result in removing the tilt; or, in other words, they convert the dispersion relation from a tilted ellipse to an untilted ellipse. Though we approach the well-posedness of PMDL from the viewpoint of rational ABCs, the ideas of variable transformations used for PML [23–30,32] and other rational ABCs [33] are similar to the one discussed previously of converting a tilted ellipse in (σ_y, σ_x) space to an untilted ellipse in $(\sigma_y, iK/\omega)$ space. However, the reference to untilted cases is made in this work purely to gain a better understanding of the inner workings of PMDL and for comparison purposes only. Note that the PMDL formulation (of approximating stiffness instead of wavenumbers) is such that *no explicit coordinate transformation is required*. This, we hope, will facilitate a relatively straightforward extension to the well-posedness studies of models involving corners and heterogeneous (layered) media; work on this is currently ongoing.

We also mention that the proof of well-posedness presented here *does not* contradict the result of [26] which, in essence, states that a necessary condition for stability of PML with complex coordinate stretching in the direction of unboundedness (x) is $c_{gx}c_{px} \geqslant 0$. The result in [26] is derived for a full-space PML medium with *constant complex* coordinate stretching; it considers the continuous, un-truncated PML. The n-layer PMDL considered here has purely imaginary layer lengths; it is discrete and truncated to begin with. Moreover, the PMDL formulation is such that there is *no* discretization error (*only* truncation error). Hence, it seems that even in the limit of fine discretization, the n-layer PMDL tends to the *truncated* continuous PML and not the full-space PML (both PML and PMDL considered with similar stretching i.e. both with complex or purely imaginary stretching). While it may seem counterintuitive, ongoing work suggests that it is this truncation that contributes to the well-posedness of PMDL. A detailed analysis is outside the scope of this paper.

5. Numerical stability

It is known that well-posedness by itself does not guarantee numerical stability. Typically well-posedness is associated with boundedness of continuous models while stability deals with their discretized counterparts. It is important to recognize that well-posedness by itself may not exclude exponential growth, but stability requirements impose no growth, or at most polynomial growth [26]. Moreover, numerical stability deals with issues arising out of numerical implementation and finite precision arithmetic. PMDL as presented till now is continuous in time but discrete in space to begin with. Hence numerical stability here refers to time discretization and finite precision arithmetic.

We are interested in asymptotic stability i.e. boundedness of the solution as $t \to \infty$. It is well-known from eigenvalue analysis that if λ denotes an eigenvalue of a matrix $\mathbf{M}$, a first order system of the form $\partial\mathbf{u}/\partial t = \mathbf{M}\mathbf{u}$ is asymptotically stable if and only if, (a) $Re(\lambda) \leqslant 0$ and (b) $Re(\lambda) = 0 \Rightarrow \lambda$ is semi-simple. Stability proof of the time discretized equations can be simplified using the results of continuous time stability presented in the following sub-section.

5.1. Continuous time stability

Inverse Fourier transforming (17) through the duality $\partial/\partial t \leftrightarrow -i\omega$, and defining $\mathbf{v} = \partial\mathbf{u}/\partial t,\ \mathbf{w} = \int \mathbf{u}dt$, we get,

$$\mathbf{F} = \mathbf{C}\mathbf{v} + \mathbf{K}\mathbf{u} + \mathbf{R}\mathbf{w}. \tag{46}$$

The matrix $\mathbf{C}$ can easily be seen to be invertible from (16). For $\mathbf{F} = \mathbf{0}$, (46) can be reformulated as,

$$\frac{\partial}{\partial t}\begin{Bmatrix}\mathbf{u}\\ \mathbf{w}\end{Bmatrix} = \begin{bmatrix}-\mathbf{C}^{-1}\mathbf{K} & -\mathbf{C}^{-1}\mathbf{R}\\ \mathbf{I} & \mathbf{0}\end{bmatrix}\begin{Bmatrix}\mathbf{u}\\ \mathbf{w}\end{Bmatrix}. \tag{47}$$

Eq. (47) is of the form $\partial\mathbf{u}/\partial t = \mathbf{M}\mathbf{u}$, and if λ are the eigenvalues, then,

$$\mathbf{0} = |\mathbf{M} - \lambda\mathbf{I}| = \begin{vmatrix}-\mathbf{C}^{-1}\mathbf{K} - \lambda\mathbf{I} & -\mathbf{C}^{-1}\mathbf{R}\\ \mathbf{I} & -\lambda\mathbf{I}\end{vmatrix} = |\lambda^2\mathbf{I} + \lambda\mathbf{C}^{-1}\mathbf{K} + \mathbf{C}^{-1}\mathbf{R}| = |\mathbf{C}^{-1}||\lambda^2\mathbf{C} + \lambda\mathbf{K} + \mathbf{R}|, \tag{48}$$

where the third equality follows from the standard block determinant of matrices simplified by the presence of the identity matrices in the lower two blocks with the assumption of $\lambda \neq 0$. Comparing (48) with (17), and noting that $|\mathbf{C}^{-1}| \neq 0$, we get $\lambda = -i\omega_R$, where ω_R are the resonant frequencies (i.e. ω_R satisfy $|-i\omega_R\mathbf{C} + \mathbf{K} + (i/\omega_R)\mathbf{R}| = 0$). Note that the assumption $\lambda \neq 0$ is now validated because $\omega_R \neq 0$.

In the previous section we proved that (45) ensured well-posedness. Trefethen and Halpern [35] have proved that a necessary condition for well-posedness is that the zeroes of $\widetilde{P}_{2n,2n-2}(\bar{\sigma}_y)/\bar{\sigma}_y$ (defined in (37)) are real and simple (Theorem 2 in [35]). Using (37), (19) and (22), the theorem regarding the zeroes of $\widetilde{P}_{2n,2n-2}(\bar{\sigma}_y)/\bar{\sigma}_y$ translates to the resonant frequencies ω_R being real and simple. This ensures asymptotic stability.

5.2. Discretized time stability

A Crank–Nicolson discretization of (47) gives,

$$\frac{1}{\Delta t}\begin{Bmatrix}\mathbf{u}_{t+\Delta t}-\mathbf{u}_t\\ \mathbf{w}_{t+\Delta t}-\mathbf{w}_t\end{Bmatrix}=\frac{1}{2}\begin{bmatrix}-\mathbf{C}^{-1}\mathbf{K} & -\mathbf{C}^{-1}\mathbf{R}\\ \mathbf{I} & \mathbf{0}\end{bmatrix}\begin{Bmatrix}\mathbf{u}_{t+\Delta t}+\mathbf{u}_t\\ \mathbf{w}_{t+\Delta t}+\mathbf{w}_t\end{Bmatrix} \tag{49}$$

From the previous subsection we know that the eigenvalues $\lambda = -i\omega_R$ of $\mathbf{M}$ are simple. Hence $\mathbf{M}$ is diagonalizable and we have $\mathbf{MV} = \mathbf{VD}$ where $D = diag\{\lambda_1,\ldots,\lambda_{2n}\}$. Using this (49) can be manipulated as follows:

$$\begin{aligned}
&\frac{1}{\Delta t}\mathbf{V}\mathbf{V}^{-1}\begin{Bmatrix}\mathbf{u}_{t+\Delta t}-\mathbf{u}_t\\ \mathbf{w}_{t+\Delta t}-\mathbf{w}_t\end{Bmatrix}=\frac{1}{2}\begin{bmatrix}-\mathbf{C}^{-1}\mathbf{K} & -\mathbf{C}^{-1}\mathbf{R}\\ \mathbf{I} & \mathbf{0}\end{bmatrix}\mathbf{V}\mathbf{V}^{-1}\begin{Bmatrix}\mathbf{u}_{t+\Delta t}+\mathbf{u}_t\\ \mathbf{w}_{t+\Delta t}+\mathbf{w}_t\end{Bmatrix}\\
&\frac{1}{\Delta t}\mathbf{V}^{-1}\begin{Bmatrix}\mathbf{u}_{t+\Delta t}-\mathbf{u}_t\\ \mathbf{w}_{t+\Delta t}-\mathbf{w}_t\end{Bmatrix}=\frac{1}{2}\mathbf{D}\mathbf{V}^{-1}\begin{Bmatrix}\mathbf{u}_{t+\Delta t}+\mathbf{u}_t\\ \mathbf{w}_{t+\Delta t}+\mathbf{w}_t\end{Bmatrix}\\
&-\left[\frac{1}{2}\mathbf{D}+\frac{1}{\Delta t}\mathbf{I}\right]\mathbf{V}^{-1}\begin{Bmatrix}\mathbf{u}_t\\ \mathbf{w}_t\end{Bmatrix}=\left[\frac{1}{2}\mathbf{D}-\frac{1}{\Delta t}\mathbf{I}\right]\mathbf{V}^{-1}\begin{Bmatrix}\mathbf{u}_{t+\Delta t}\\ \mathbf{w}_{t+\Delta t}\end{Bmatrix}
\end{aligned} \tag{50}$$

Since $\mathbf{D}$ is diagonal, the last system in (50) is a set of decoupled equations of the general form,

$$\phi_{t+\Delta t}=\left(\frac{1/\Delta t+\lambda/2}{1/\Delta t-\lambda/2}\right)\phi_t=\left(\frac{2+\lambda\Delta t}{2-\lambda\Delta t}\right)\phi_t \tag{51}$$

with ϕ denoting *any* component of the vector $\mathbf{V}^{-1}\{\mathbf{u}\ \mathbf{w}\}^T$ and λ the corresponding eigenvalue. Since $\lambda = -i\omega_R$, we have $|\phi_{t+\Delta t}| = |\phi_t|$. This implies asymptotic stability of the time discretized form (49). Note that (46) models only the exterior and hence the numerical stability assured by (51) does not consider the effect of the interior on the stability of the coupled (interior + exterior) model. As mentioned before, we do not consider issues related to interior discretization in this work. We mention however, that in the presence of an interior, time discretization is performed using the implicit extended constant average acceleration (instead of Crank–Nicolson) and details of its implementation can be found in [38,45,49].

5.3. Finite precision issues

While (51) ensures asymptotic stability, it still neglects issues related to finite precision arithmetic. While the theorem of Trefethen and Halpern (Theorem 2 in [35]) ensures that the resonant frequencies are simple (and hence distinct), they can be arbitrarily close to each other, especially for large number of layers. If round off errors due to finite precision make these frequencies indistinguishable, there will be polynomial growth associated with repeated eigenvalues. In the case of multiple

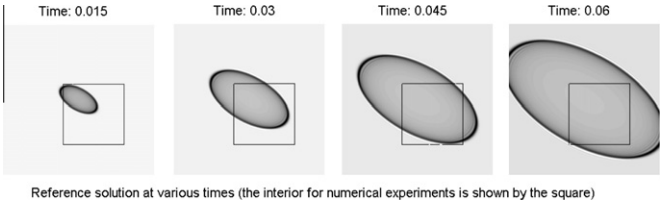

Fig. 5. Reference solution in a large (500 × 500) domain at various times. For numerical experiments, the interior chosen is denoted by the square and PMDL is applied at the edges of this square.

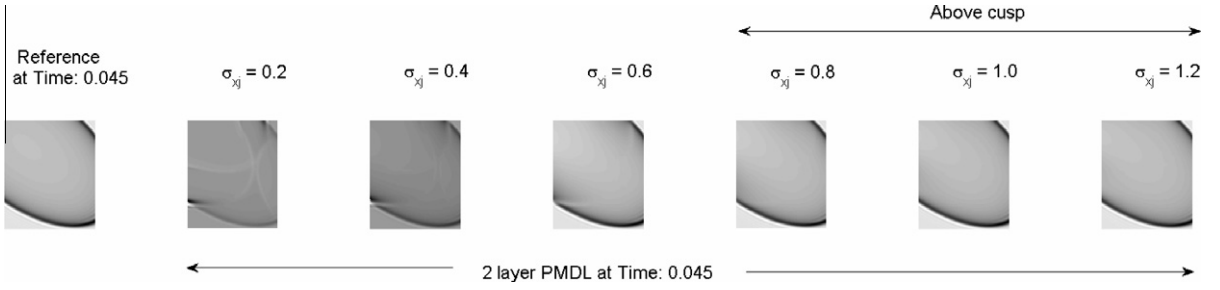

Fig. 6. Interior solution for a 2 layer PMDL exterior with various PMDL parameters. Only the last three simulations have parameters above the cusp and thus satisfy the well-posedness and accuracy criterion.

absorbing boundaries, this can also manifest as exponential growth [48]. The variable in (51) is also not the original field variable $\{\mathbf{u}\ \mathbf{w}\}^T$, but $\mathbf{V}^{-1}\{\mathbf{u}\ \mathbf{w}\}^T$. In the presence of $\mathbf{V}^{-1}$, the magnitude of the field variables will depend on the condition number of $\mathbf{V}$ which may be large. Moreover, $\lambda = -i\omega_R$ only ensures $Re(\lambda) = 0$ and not the stronger form $Re(\lambda) < 0$. Numerical perturbations due to finite precision arithmetic may result in $Re(\lambda) > 0$ and this implies growth in time. Finite precision issues are beyond the scope of this work.

6. Numerical examples

We consider a 2D model problem with a square interior consisting of a scalar tilted anisotropic medium that is modeled by a mesh of 200×200 regular square bilinear finite elements of size $h = 2 \times 10^{-4}$. The exterior is represented by ABCs on all four edges/corners. Using the material parameters $a = 1$, $b = 2$, $\beta = 30°$ in (3), the well-posedness and accuracy condition for PMDL in the x direction is $\sigma_{xj} > 0.72$ (45). For PMDL in the y direction we have $a = 1$, $b = 2$, $\beta = 60°$ and hence (45) results in $\sigma_{yj} > 0.98$. For simplicity, we assume $\sigma_{yj} = 1.5\sigma_{xj}$ and $\sigma_{x1} = \sigma_{x2} = \ldots = \sigma_{xn}$, thus reducing the number the PMDL parameters to just one. The excitation is assumed to be $\sin^2(\pi x/5h) \times \sin^2(\pi y/5h) \times \sin^2(\pi t/10\Delta t)$ for $|x| \leqslant 5h$, $|y| \leqslant 5h$ and $t \leqslant 10\Delta t$ where $\Delta t = 2 \times 10^{-4}$ is the time step size. The excitation is taken to occur at the origin of the coordinate system with the four corners of the interior domain being positioned at $(-0.01, 0.01)$, $(0.03, 0.01)$, $(0.03, -0.03)$ and $(-0.01, -0.03)$. This ensures that the excitation is at the center of the upper left quarter of the interior i.e. it is placed closer to some interior boundaries and corners than others. For comparison, the reference solution is obtained using a 500×500 interior with the same element and

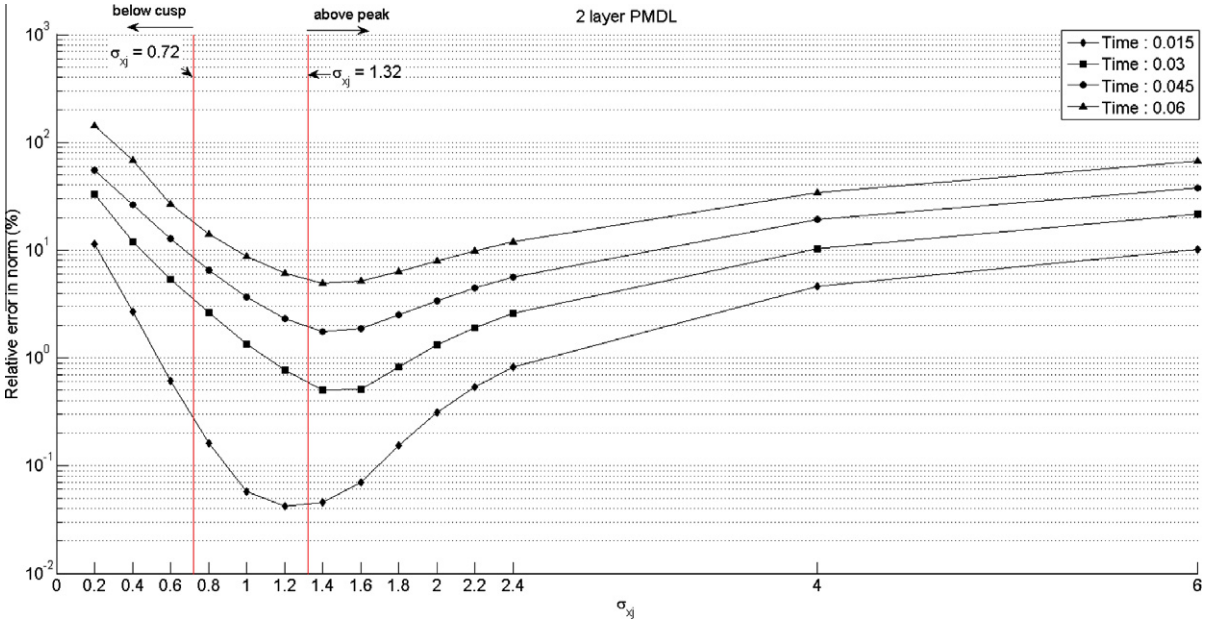

Fig. 7. Relative error in norm for a 2 layer PMDL with various parameters at different times. The lines demarcating the cusp of the slowness ellipse and its peak are shown.

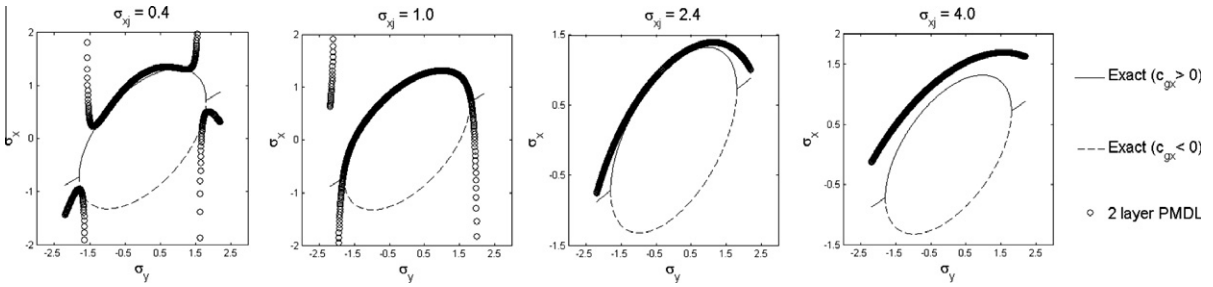

Fig. 8. Slowness diagrams for 2 layer PMDL approximation with parameters chosen below the cusp, between the cusp and peak and above the peak. The first figure has interpolation points with negative group velocity while the second one has interpolation points with positive group velocity. The last two do not have any interpolation points on the ellipse though they do approximate only the positive group velocity branch.

time step size as before. The relative error in norm is calculated as $\|u_{\text{PMDL}} - u_{\text{reference}}\|_2 / \|u_{\text{reference}}\|_2$ and expressed as a percentage. The interior chosen and the reference solution at various times is shown in Fig. 5.

The accuracy obtained for different values of the PMDL parameters σ_{xj} for a 2 layer PMDL can be visually inferred from Fig. 6 and is numerically quantified in Fig. 7. The inaccuracies of violating (45) are obvious in Figs. 6 and 7 shows that the least accurate results are obtained when σ_{xj} is below the cusp i.e. when the parameters violate the accuracy and well-posedness criterion (45). In the present case (45) implies $\sigma_{xj} > 0.72$ and since we use $\sigma_{yj} = 1.5\sigma_{xj}$, (45) is also violated in the y direction when $\sigma_{xj} = 0.2, 0.4, 0.6$. The relative error is also seen to increase when the parameters are chosen above the peak of the ellipse. This is because of the fact that for such parameters there will be no interpolation points on the ellipse (see [40]) and

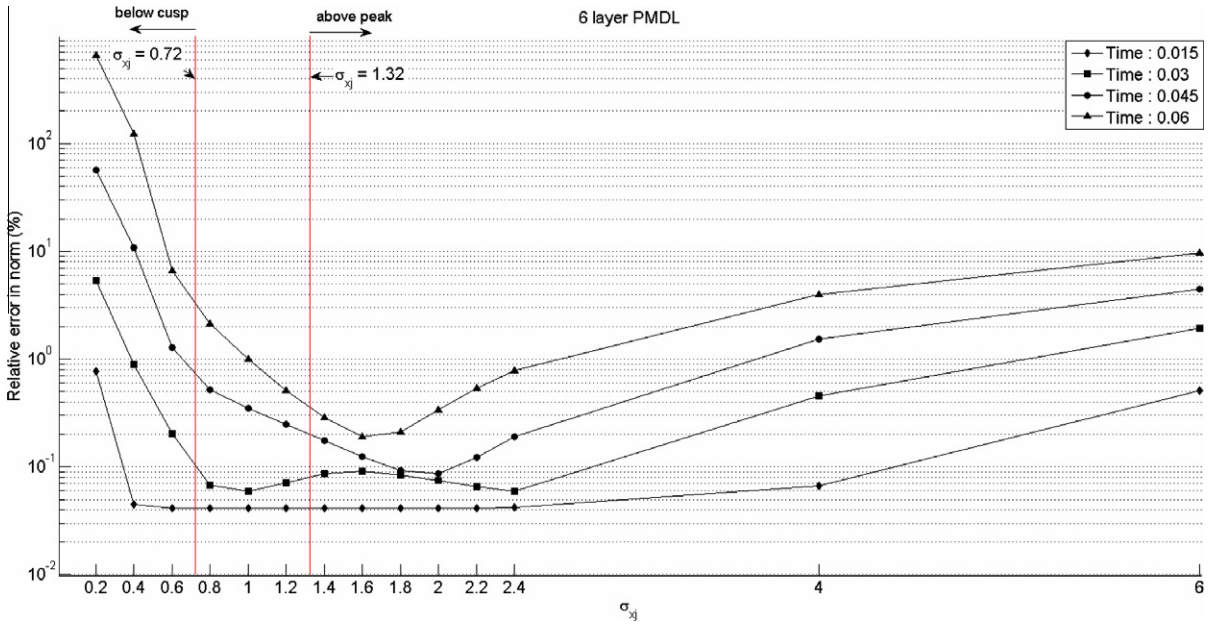

Fig. 9. Relative error in norm for a 6 layer PMDL with various parameters. The lines demarcating the cusp of the slowness ellipse and its peak are shown.

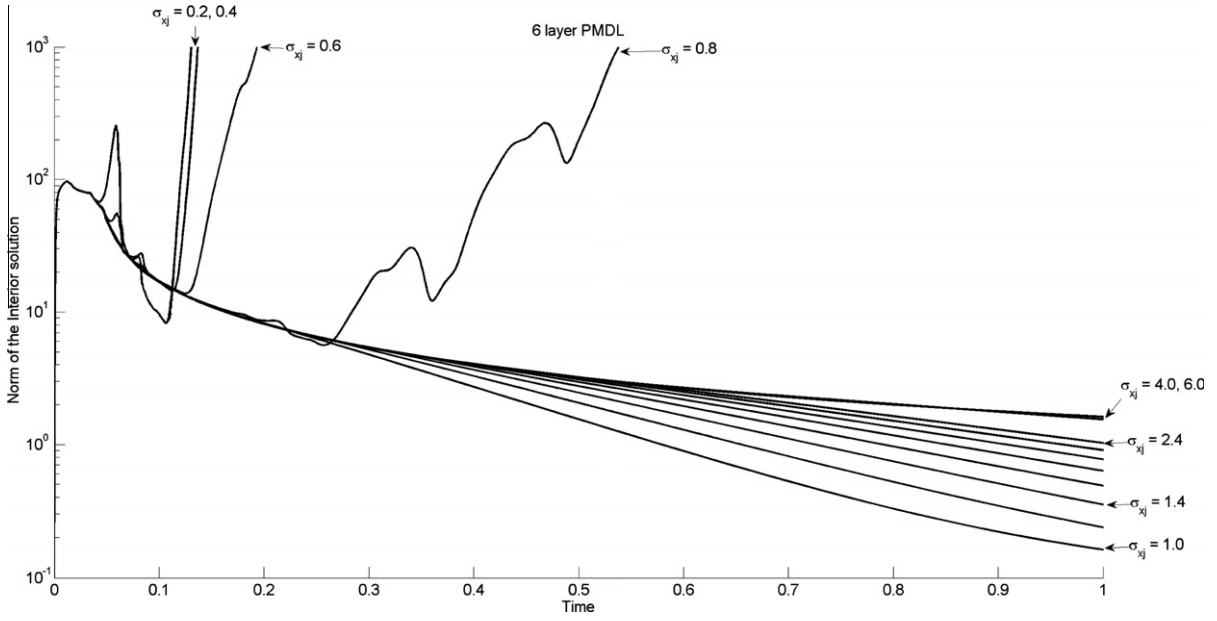

Fig. 10. Long time behavior of the interior solution with a 6 layer PMDL approximating the exterior with various parameters.

since we wish to capture a part of the ellipse (the positive group velocity part) we should expect some loss in accuracy in this case. The slowness diagram from [40] is presented again in Fig. 8 to clarify this point.

Increasing the number of PMDL layers will improve the accuracy *only if* the parameters satisfy (45). This is clearly demonstrated in Fig. 9. By comparing Figs. 7 and 9, we see that for parameters chosen below the cusp, there is an improvement in accuracy only at earlier times. With increasing time, and hence with increasing number of reflections from the PMDL boundaries, the solution deteriorates. The gain in accuracy when parameters satisfying (45) are chosen is also evident from these two figures.

The importance of (45) on the well-posedness and stability of the problem at hand is demonstrated by examining the long time behavior of the numerical solution. Fig. 10 shows that except for the case of $\sigma_{xj} = 0.8$, instability occurs *only* when the parameters violate (45) i.e. when $\sigma_{xj} \leqslant 0.72$ and the solution is stable when (45) is satisfied.

The case of $\sigma_{xj} = 0.8$ becoming unstable even while satisfying (45) can be explained by observing the interior solution shown in Fig. 11. It was noted that when parameters are chosen above the cusp and very near to it, such instability occurs when the number of PMDL layers is large. For example it does not occur with a 2 layer PMDL. For a 6 layer PMDL, Fig. 11 shows ripples along the boundary that are characteristic of this kind of instability. These ripples decay exponentially in a direction perpendicular to the boundary and propagate along the boundary with their amplitudes increasing with time. This suggests that they are due to a combination of the reflection of evanescent waves not handled by the PMDL used in this experiment and the highly oscillatory behavior of the PMDL approximation near the zero group velocity regions of the slowness diagram (see [40]). Such an instability can be handled as in [40] by either not using parameters very near the cusp or by using padding layers between the interior and PMDL. The effect of using parameters relatively far from the cusp is evident in

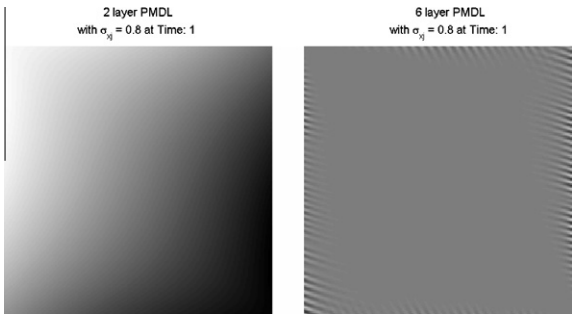

Fig. 11. Interior solution for the case where the PMDL parameter is above the cusp but still close to it.

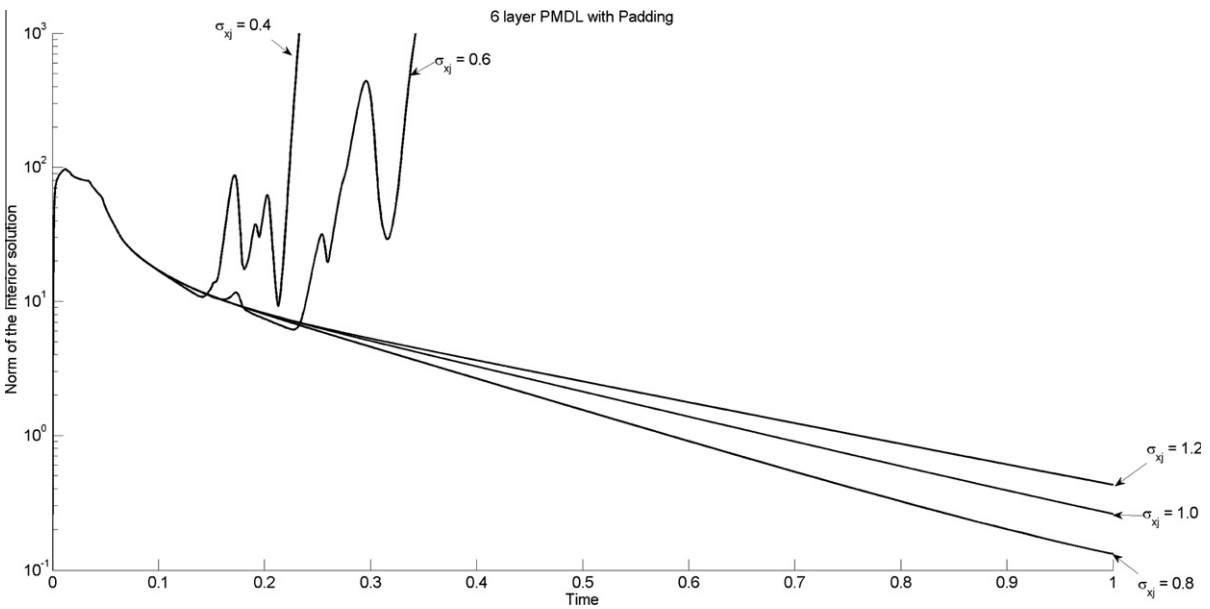

Fig. 12. Long time behavior of the interior solution with a 6 layer PMDL approximating the exterior with parameters chosen near the cusp. The rogue behavior seen with $\sigma_{xj} = 0.8$ in Fig. 10 is no longer present. Six padding layers with ad hoc parameters were used.

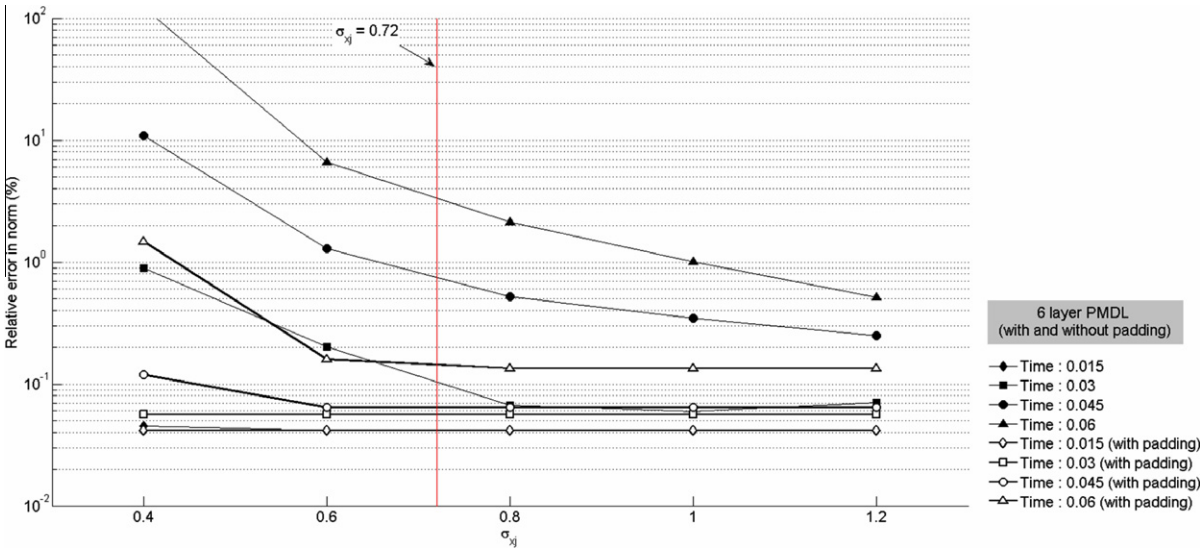

Fig. 13. Comparison of accuracy achieved with and without padding layers. The gain in accuracy can be attributed to the handling of the evanescent spectrum and the smoothening of the PMDL approximation near zero group velocity modes.

Fig. 10. Padding layers are a form of PMDL that can handle evanescent waves and consist of mid-point integrated linear finite elements with real lengths [44,45]; without delving into the behavior and design of padding layers, we present the effect of PMDL with padding in Figs. 12 and 13. When compared to Fig. 10, Fig. 12 clearly shows the stabilization of the $\sigma_{xj} = 0.8$ case. While the experiments with the correct parameters lead to stable solutions, their accuracy can be seen to reduce with time both in Fig. 10 and in Fig. 12. This loss in long term accuracy is consistent with the observation in [10] and can be attributed to the fact that we have either completely neglected the evanescent spectrum or only handled it in an ad hoc manner. We reemphasize that PMDL *can* handle evanescent modes effectively [44,45]; our restriction to propagating modes is intended only to make the well-posedness problem tractable. Unlike in the case of [45], the behavior of padding layers in the case of tilted anisotropic acoustics is not completely understood yet and the padding layers may only be delaying the onset of instability (instead of completely eliminating it). Their use here to handle instabilities is based on promising but preliminary studies.

7. Summary and conclusions

A necessary and sufficient condition for well-posedness of PMDL is presented for the scalar anisotropic wave equation. This condition also turns out to be sufficient for accuracy. The algebraic criterion derived here provides a simple bound for PMDL layer lengths and ensures well-posedness in Kreiss's sense. This bound depends on the anisotropy of the medium, in particular the tilt, and guarantees strong well-posedness of any PMDL satisfying the bound.

The final form of the well-posed PMDL derived here is similar to the well-posed PML [23–30,32] and rational ABC [33] obtained through coordinate rotations, but has two important differences: (a) Well-posedness analyses of PML typically consider full-space IVPs, while we consider the IBVPs obtained from coupling the interior with truncated PMDL. (b) Existing analyses consider continuous PMLs, while we consider PMDL, which is already a discretized version of PML, with the important property of perfect matching even after discretization. Thus, the problem considered in this paper is closer to the computational problem which involves both discretization and truncation (although we do not consider the issue of *interior* discretization).

To make the well-posedness problem tractable, the PMDL formulation is not considered in all its generality. The present study is confined to propagating wave modes, single straight computational boundary and homogeneous though anisotropic exteriors. None of the these restrictions, however, are due to actual limitations of PMDL and the PMDL formulation shows promise of being extendible to more complex media. For instance, in deriving the well-posedness criterion, the PMDL formulation is shown to naturally overcome challenges posed by the existence of wave modes with differing phase and group velocity signs *without the need of an explicit coordinate transformation.* This is unlike the techniques used to handle opposing phase and group velocity signs for the design of both PMLs [23–30,32] and rational ABCs [33]. Since techniques involving coordinate rotations cannot be directly extended to heterogeneous (layered) media, the PMDL ABC holds greater promise for such media. Moreover, the distinctive property of PMDL, namely approximation of half-space stiffness instead of the wavenumber, is central to the ability of PMDL to capture the correct group velocities even when the group and phase velocities are not aligned in the same direction. This is because the group velocity and stiffness are related (at least in this case) and PMDL approximates the stiffness. We hypothesize that the link between group velocity and stiffness extends to general

vector systems and that this link can be used to ensure well-posedness of PMDL even in more complicated media (like elastodynamics) that are governed by vector equations. Further investigation in this direction is underway.

References

[1] D. Givoli, Nonreflecting boundary-conditions, J. Comput. Phys. 1 (1991) 1–29.
[2] S.V. Tsynkov, Numerical solution of problems on unbounded domains. A review, Appl. Numer. Math. 4 (1998) 465–532.
[3] T. Hagstrom, New results on absorbing layers and radiation boundary conditions, Topics in Computational Wave Propagation – Direct and Inverse Problems (2003) 1–42.
[4] E.L. Lindman, Free-space boundary-conditions for time-dependent wave-equation, J. Comput. Phys. 1 (1975) 66–78.
[5] B. Engquist, A. Majda, Absorbing boundary-conditions for numerical-simulation of waves, Math. Comput. 139 (1977) 629–651.
[6] B. Engquist, A. Majda, Radiation Boundary-conditions for acoustic and elastic wave calculations, Commun. Pure Appl. Math. 3 (1979) 313–357.
[7] A. Bayliss, E. Turkel, Radiation boundary-conditions for wave-like equations, Commun. Pure Appl. Math. 6 (1980) 707–725.
[8] R.L. Higdon, Numerical absorbing boundary-conditions for the wave-equation, Math. Comput. 179 (1987) 65–90.
[9] D. Givoli, High-order local non-reflecting boundary conditions: a review, Wave Motion 4 (2004) 319–326.
[10] T. Hagstrom, A. Mar-Or, D. Givoli, High-order local absorbing conditions for the wave equation: extensions and improvements, J. Comput. Phys. 6 (2008) 3322–3357.
[11] J.P. Bérenger, A perfectly matched layer for the absorption of electromagnetic-waves, J. Comput. Phys. 2 (1994) 185–200.
[12] W.C. Chew, J.M. Jin, E. Michielssen, Complex coordinate stretching as a generalized absorbing boundary condition, Microwave Opt. Technol. Lett. 6 (1997) 363–369.
[13] W.C. Chew, W.H. Weedon, A 3D perfectly matched medium from modified Maxwells equations with stretched coordinates, Microwave Opt. Technol. Lett. 13 (1994) 599–604.
[14] Z.S. Sacks, D.M. Kingsland, R. Lee, J.F. Lee, A perfectly matched anisotropic absorber for use as an absorbing boundary condition, IEEE Trans. Antennas Propag. 12 (1995) 1460–1463.
[15] F.L. Teixeira, W.C. Chew, Analytical derivation of a conformal perfectly matched absorber for electromagnetic waves, Microwave Opt. Technol. Lett. 17 (1998) 231–236.
[16] Kuzuoglu, Mittra, Frequency dependence of the constitutive parameters of causal perfectly matched anisotropic absorbers, IEEE Microwave Guided Wave Lett. 12 (1996) 447.
[17] Roden, Gedney, Convolution PML (CPML): an efficient FDTD implementation of the CFS-PML for arbitrary media, Microwave Opt. Technol. Lett. 5 (2000) 334.
[18] Meza-Fajardo, Papageorgiou, A nonconvolutional, split-field, perfectly matched layer for wave propagation in isotropic and anisotropic elastic media: Stability analysis. Bulletin of the Seismological Society of America 4 (2008) 1811–1836.
[19] S. Abarbanel, D. Gottlieb, A mathematical analysis of the PML method, J. Comput. Phys. 2 (1997) 357–363.
[20] J.S. Hesthaven, On the analysis and construction of perfectly matched layers for the linearized Euler equations, J. Comput. Phys. 1 (1998) 129–147.
[21] P.G. Petropoulos, L. Zhao, A.C. Cangellaris, A reflectionless sponge layer absorbing boundary condition for the solution of Maxwell's equations with high-order staggered finite difference schemes, J. Comput. Phys. 1 (1998) 184–208.
[22] Feng, Absorbing boundary conditions for electromagnetic wave propagation, Math. Comput. 225 (1999) 145.
[23] S. Abarbanel, D. Gottlieb, J.S. Hesthaven, Well-posed perfectly matched layers for advective acoustics, J. Comput. Phys. 2 (1999) 266–283.
[24] F.Q. Hu, A stable, perfectly matched layer for linearized Euler equations in unsplit physical variables, J. Comput. Phys. 2 (2001) 455–480.
[25] T. Hagstrom, A new construction of perfectly matched layers for hyperbolic systems with applications to the linearized Euler equations, in: Cohen et al. (Ed.), Mathematical and numerical aspects of wave propagation, Proceedings Waves 2003, Springer-Verlag, 2003, pp. 125–129.
[26] E. Bécache, S. Fauqueux, P. Joly, Stability of perfectly matched layers, group velocities and anisotropic waves, J. Comput. Phys. 2 (2003) 399–433.
[27] E. Bécache, A.S. Bonnet-Ben Dhia, G. Legendre, Perfectly matched layers for the convected Helmholtz equation, SIAM J. Numer. Anal. 1 (2004) 409–433.
[28] F.Q. Hu, A perfectly matched layer absorbing boundary condition for linearized Euler equations with a non-uniform mean flow, J. Comput. Phys. 208 (2005) 469–492.
[29] E. Bécache, A.S.B.B. Dhia, G. Legendre, Perfectly matched layers for time-harmonic acoustics in the presence of a uniform flow, SIAM J. Numer. Anal. 3 (2006) 1191–1217.
[30] J. Diaz, P. Joly, A time domain analysis of PML models in acoustics, Comput. Methods Appl. Mech. Eng. 29–32 (2006) 3820–3853.
[31] D. Appelö, G. Kreiss, A new absorbing layer for elastic waves, J. Comput. Phys. 2 (2006) 642–660.
[32] S. Parrish, F. Hu, PML absorbing boundary conditions for the linearized and nonlinear Euler equations in the case of oblique mean flow, Int. J. Numer. Methods Fluids 60 (2009) 565–589.
[33] E. Becache, D. Givoli, T. Hagstrom, High-order absorbing boundary conditions for anisotropic and convective wave equations, J. Comput. Phys. 229 (2010) 1099–1129.
[34] R.L. Higdon, Initial-boundary value-problems for linear hyperbolic systems, SIAM Rev. 2 (1986) 177–217.
[35] L.N. Trefethen, L. Halpern, Well-posedness of one-way wave-equations and absorbing boundary-conditions, Math. Comput. 176 (1986) 421–435.
[36] D. Appelö, T. Hagstrom, G. Kreiss, Perfectly matched layers for hyperbolic systems: general formulation, well-posedness, and stability, SIAM J. Appl. Math. 1 (2006) 1–23.
[37] K.W. Lim, Absorbing boundary conditions for corner regions, Master's Thesis, North Carolina State University, 2003.
[38] M.N. Guddati, K.W. Lim, Continued fraction absorbing boundary conditions for convex polygonal domains, Int. J. Numer. Methods Eng. 6 (2006) 949–977.
[39] M.N. Guddati, K.W. Lim, M.A. Zahid, Perfectly matched discrete layers for unbounded domain modeling, in: F. Magoulès (Ed.), Computational Methods for Acoustics Problem, Saxe-Coburg Publications, Scotland, 2008, pp. 69–98.
[40] S. Savadatti, M.N. Guddati, Absorbing boundary conditions for scalar waves in anisotropic media. Part 1: Time harmonic modeling, J. Comput. Phys., 2010, in press, doi:10.1016/j.jcp.2010.05.018.
[41] H.O. Kreiss, Initial boundary value problems for hyperbolic systems, Commun. Pure Appl. Math. 3 (1970). 277–&.
[42] H. Kreiss, J. Lorenz, Initial-Boundary Value Problems and the Navier–Stokes Equations, Academic Press, Boston, 1989. p. 402.
[43] S. Asvadurov, V. Druskin, M.N. Guddati, L. Knizhnerman, On optimal finite-difference approximation of PML, SIAM J. Numer. Anal. 1 (2003) 287–305.
[44] M.N. Guddati, Arbitrarily wide-angle wave equations for complex media, Comput. Methods Appl. Mech. Eng. 1–3 (2006) 65–93.
[45] M.A. Zahid, M.N. Guddati, Padded continued fraction absorbing boundary conditions for dispersive waves, Comput. Methods Appl. Mech. Eng. 29–32 (2006) 3797–3819.
[46] T. Hagstrom, T. Warburton, Complete radiation boundary conditions: minimizing the long time error growth of local methods, <http://faculty.smu.edu/thagstrom/HWcomplete.pdf>, 2008.
[47] R.L. Higdon, Absorbing boundary-conditions for difference approximations to the multidimensional wave-equation, Math. Comput. 176 (1986) 437–459.
[48] L.N. Trefethen, Group-Velocity interpretation of the stability theory of Gustafsson, Kreiss, and Sundstrom, J. Comput. Phys. 2 (1983) 199–217.
[49] M.N. Guddati, J.L. Tassoulas, Continued-fraction absorbing boundary conditions for the wave equation, J. Comput. Acoust. 1 (2000) 139–156.